SUMOylation of Jun fine-tunes the *Drosophila* gut immune response

Amarendranath Soory & Girish Ratnaparkhi

Department of Biology, Indian Institute of Science Education & Research, Pune 411008, INDIA

Author for Correspondence: girish@iiserpune.ac.in

Address:

Biology, Indian Institute of Science Education & Research (IISER)

Dr. Homi Bhabha Road, Pashan, Pune 411008, INDIA

Phone: +91-20-2590-8053

ORCID IDs: AS (0000-0003-3023-6121), GR (0000-0001-7615-3140)

Running Title: Conjugation of Jun by SUMO regulates gut immunity

ABSTRACT

Post-translational modification by the small ubiquitin-like modifier, SUMO can modulate the activity of its conjugated proteins. The transcriptional regulator Jun, a member of the AP-1, complex is one such SUMO target. We find that Jra, the *Drosophila* Jun ortholog, is a regulator of the *Pseudomonas entomophila* induced gut immune gene regulatory network, modulating the expression of a few thousand genes, as measured by quantitative RNA sequencing. Decrease in *Jra* in gut enterocytes is protective, suggesting that reduction of Jra signaling favors the host over the pathogen. In Jra, lysines 29 and 190 are SUMO conjugation targets, with the $Jra^{K29R+K190R}$ double mutant being SUMO conjugation resistant (SCR). Interestingly, a Jra^{SCR} fly line, generated by CRISPR/Cas9 based genome editing, is more sensitive to infection, with adults showing a weakened host response and increased proliferation of *Pseudomonas.* Transcriptome analysis of the guts of Jra^{SCR} and Jra^{WT} flies suggests that lack of SUMOylation of Jra significantly changes core elements of the immune gene regulatory network, that include antimicrobial agents, secreted ligands, feedback regulators, and transcription factors. SUMOylation attenuates Jra activity, with the master immune regulator Relish being an important transcriptional target. Our study implicates Jra as a major immune regulator, with dynamic SUMO conjugation/deconjugation modulating the kinetics of the gut transcriptional immune response.

Keywords

NFκB, *Pseudomonas*, Enterocytes, infection, SUMO, Jra, AP-1

44 **INTRODUCTION**

45 Proteins undergo post-translational modifications (PTM) by reversible and covalent
46 attachment of a diverse set of molecules. PTMs can modulate the target protein's structure,
47 stability, interactions, or location and alter its function. This modulation increases the
48 complexity and diversity of a proteome. The effect of the PTM on the target protein is usually
49 context-dependent, with the combination of different PTMs affecting function in a
50 differential manner. PTMs come in all shapes and sizes with a wide variety of chemical groups.
51 One common PTM is the conjugation of one protein to another. The best-known examples of
52 such protein modifiers are Ubiquitin-like proteins (UBLs) (VAN DER VEEN AND PLOEGH 2012;
53 VIERSTRA 2012; EIFLER AND VERTEGAAL 2015; CAPPADOCIA AND LIMA 2018), a large group of proteins
54 exhibiting a Ubiquitin fold. These, along with Ubiquitin, include Nedd8, ISG15, SUMO,
55 ATG8/12, and many others. These protein PTMs conjugate a wide variety of proteins, usually
56 targeting lysine side chains.

57 The small ubiquitin-like modifier, SUMO (MELCHIOR 2000; MULLER *et al.* 2001; HAY 2005)
58 can be reversibly and covalently conjugated to a target protein. For conjugation, the
59 translated SUMO protein is made conjugation-competent by proteolytic cleavage of the C-
60 terminal tail of SUMO, exposing a –GG dipeptide. The SUMO-GG is then picked up by the
61 SUMO activating enzymes (SAEs) which transfer the SUMO to the SUMO conjugase Ubc9.
62 Ubc9 interacts with the target protein and works to attach the C-terminal GG-COO- to a lysine
63 side chain, on the target protein, via an isopeptide bond (FLOTHO AND MELCHIOR 2013; CELEN AND
64 SAHIN 2020). The conjugation is reversible and requires deconjugating enzymes (HICKEY *et al.*
65 2012). Ubc9, during conjugation, can be assisted by one or multiple SUMO ligases, which are
66 believed to provide specificity and enhance conjugation.

67 Our laboratory is interested in the role of SUMO conjugation of proteins during an
68 innate immune response in flies (HANDU *et al.* 2015; HEGDE *et al.* 2020). A subset of proteins
69 involved in immune regulatory networks are known to be SUMOylated both in vertebrates or
70 invertebrates (HANNOUN *et al.* 2016; ADORISIO *et al.* 2017; HEGDE *et al.* 2020). Our approach to
71 the problem was first to identify proteins that changed their SUMOylation status on infection.
72 We used quantitative proteomics to identify a set of proteins whose SUMOylation state either
73 increased or decreased with infection (HANDU *et al.* 2015). One SUMO target uncovered in our
74 quantitative proteomics screen (HANDU *et al.* 2015) is the *Drosophila* c-Jun ortholog Jra
75 (Flybase ID, FBgn0001291) - the Jun related antigen (PERKINS *et al.* 1988; SLUSS *et al.* 1996). Jra

76 is one of the transcriptional effectors of the JNK (Jun N-terminal kinase) signaling pathway,
77 the other being Kayak (Kay, ortholog of c-Fos) (NOSELLI 1998; NOSELLI AND AGNÈS 1999). Jra
78 function has been uncovered in multiple developmental contexts (BOHMANN *et al.* 1994;
79 RIESGOESCOVAR AND HAFEN 1997; KOCKEL *et al.* 2001; RIOS-BARRERA AND RIESGO-ESCOVAR 2013), as
80 well as in the adult animal (BITEAU *et al.* 2011; LA MARCA AND RICHARDSON 2020). The JNK kinase
81 cascade has been broadly classified as a 'stress' pathway in organisms, and our current
82 research focuses on its role in immune signaling.

83 In this study, we have explored roles for SUMO conjugation of Jra in the gut immune
84 response. Using the loss of function genetics, in combination with quantitative RNA
85 sequencing, we find that Jra is a major regulator of the genes involved in the gut immune
86 response, triggered by oral *Pseudomonas entomophila* (*Pe*) infection. Our data suggest that
87 Jra is part of an extensive immune Gene regulatory network (i-GRN) and is crucial for evoking
88 a robust immune response and maintain gut immune homeostasis. We find that SUMO
89 conjugates Jra at lysines 29 and 190, and a $Jra^{K29R+190R}$ mutant is SUMO-conjugation resistant
90 (SCR). The Jra^{SCR} double mutant line, generated by CRISPR Cas9 genome editing, is sensitive
91 to *Pe* infection and carries a higher load of bacteria, suggesting that the absence of Jra
92 SUMOylation weakens the ability of the host to resist infection. At the level of transcription,
93 lack of Jra SUMOylation changes the kinetics of the immune response, delaying and
94 weakening the activation of defense genes, an important example being the NFκB factor
95 Relish (Rel).

96 Our study thus uncovers Jra as a major transcriptional regulator of the gut immune
97 response. Increased Jra signaling appears to favor *Pseudomonas*, while SUMOylation of Jra
98 favors the host, presumably by enhancing the host response to pathogens. Thus, we postulate
99 that SUMOylation of Jra fine-tunes the host transcriptional response to infection.
100

101 RESULTS

102 ***Jra is a target for SUMO conjugation***

103 We initiated our studies by validating our initial observation (HANDU *et al.* 2015) that
104 Jra is SUMO conjugated (SUMOylated). Jra SUMOylation was validated using a previously
105 described *in-bacto* approach (NIE *et al.* 2009). Here, Jra was co-expressed in bacteria with
106 *Drosophila* SAE1, SAE2, Ubc9, and mature 6XHis-tagged SUMO (SUMO-GG) to facilitate target
107 SUMOylation. Affinity purification using glutathione beads, followed by western blotting, was
108 used to detect SUMOylated species migrating at a higher molecular weight than Jra, based on
109 the degree of conjugation. A similar experiment with an immature/dead 6XHis-tagged SUMO
110 (SUMO-ΔGG) served as a negative control. We consistently find two high molecular weight
111 bands that correspond to 1X and 2X SUMO conjugated species in the Western blots (Fig. 1A),
112 confirming that Jra is a target of SUMO conjugation. We also find a third higher molecular
113 weight band corresponding to >3X SUMO conjugated species. To discover the lysine residues
114 that are targets of SUMO machinery, we used the web-based tool, Joined Advanced
115 SUMOylation Site and Sim Analyser (JASSA) (BEAUCLAIR *et al.* 2015) to predict the putative
116 SUMO sites (Fig. 1B). SUMO is known to prefer lysine residues that follow the broad
117 consensus SUMO motif (ψ**K**XE/D), where ψ is a hydrophobic residue. A total of seven sites
118 (Fig. 1B) were targeted based both on JASSA predictions and the evolutionary conservation
119 of SUMO sites. Of these, K214 was a strong consensus motif while K29 and K190 were part of
120 Negatively charged amino acid-dependent SUMOylation (NSDM) site and Synergy Control
121 (SC) – SUMO motifs, respectively (Fig. 1C). The three-dimensional structures of Jun available
122 in the Protein Data Bank do not include the N-terminal and C-terminal regions, with secondary
123 structure predictions (MITCHELL *et al.* 2019) suggesting that K29 and K190 are in unstructured
124 regions. We replaced each of the predicted lysine residues, one at a time, with an arginine
125 residue, whose side chain is resistant to SUMO conjugation (Fig. 1D & E). Our goal was to
126 identify SUMO conjugation sites and generate a SUMO conjugation resistant mutant (SCR) of
127 Jra. Of the seven site-directed mutants tested (Fig. 1C, D and E), only two, K190R and K29R,
128 showed partial loss of SUMOylation. There were changes in the intensity of SUMOylated
129 bands for the remaining single mutations, but their SUMOylation status was maintained (Fig.
130 1D & E). As a further step to generate a Jra SCR mutant, we cloned and tested the Jra double
131 mutant, $Jra^{K29R+K190R}$. Interestingly, we found that the double mutant could not be SUMO
132 conjugated, with all three SUMOylation bands missing (Fig. 1F).

133

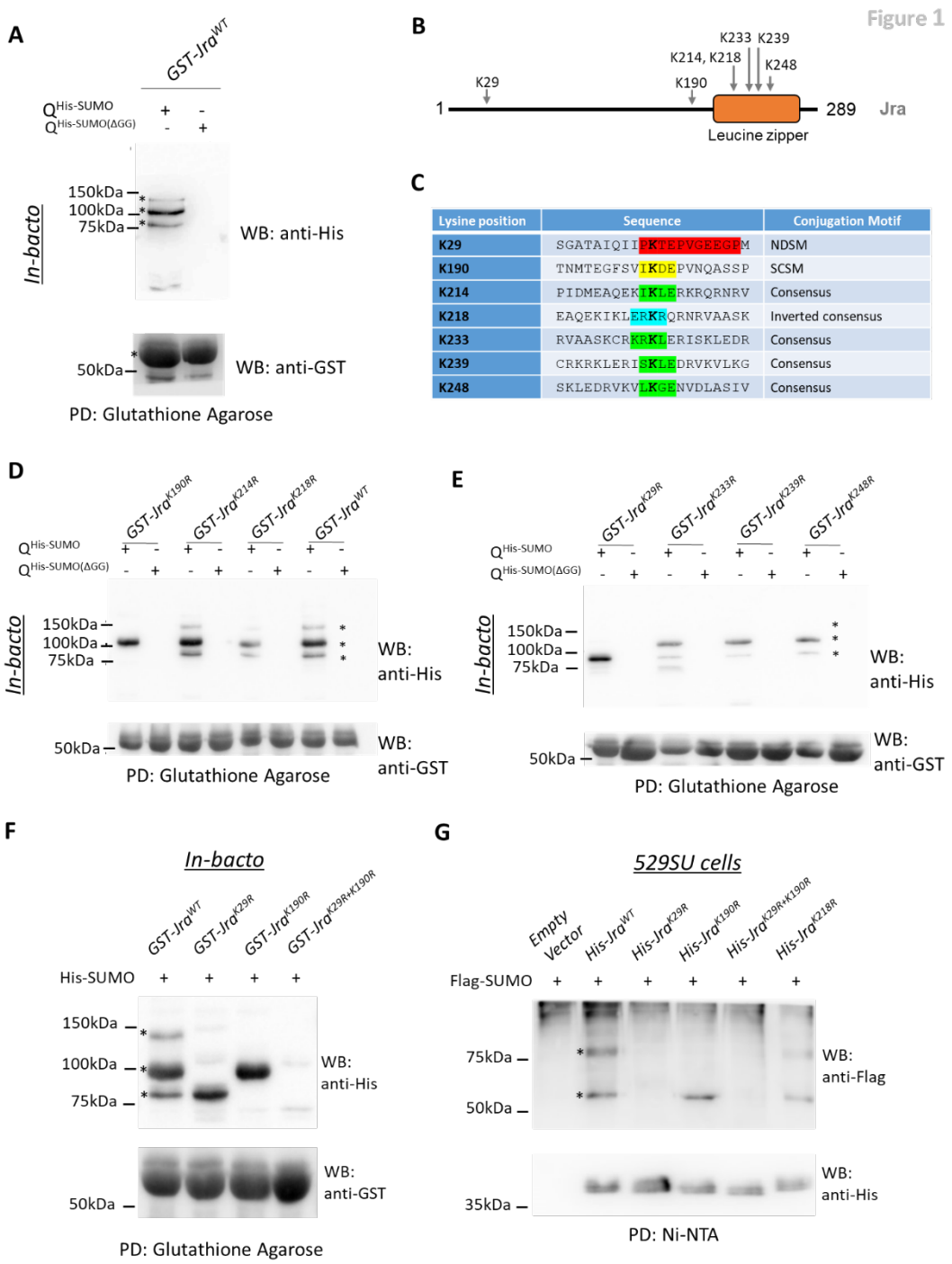

134

135 **Figure 1: Site-directed lysine mutagenesis screen identifies Jra(K29) and Jra(K190) as acceptor sites for**
136 **SUMOylation,**
137 **A.** Anti-His western blot (upper panel) post Glutathione agarose affinity pulldown (PD) shows three SUMOylated
138 bands for GST-Jra. *GST-Jra*^{WT} co-transformed with immature *SUMO (SUMO-ΔGG)* serves as a negative control for
139 SUMO conjugation. Anti-GST WB (lower panel) post affinity PD indicates similar levels of expression of GST-Jra^{WT}
140 for the experimental and control lysates.
141 **B.** Schematic of the primary sequence of *Drosophila* Jra. The conjugation sites to be tested (panel C) are mapped
142 onto Jra. Secondary structure prediction indicates that the Jra N-terminus is unstructured (black line), while the
143 C-terminus (residues 210-275) is helical. This is in agreement with structures deposited in the Protein Data Bank

(PDB:1FOS), which correspond only to the C-terminal leucine zipper (orange box), formed from c-Jun/c-Fos dimers.

C. Putative SUMO motifs predicted for Jra include the negative amino-acid dependant SUMO motif (NDSM; K29), synergy consensus SUMO motif (SCSM; K190), four consensus SUMO motifs (K214, K233, K239 and K248) and an inverted consensus motif (K218).

D. Anti-His western blot (upper panel) post PD showing the SUMOylated bands of Jra and its mutant variants. Jra^{K190R} shows partial loss of SUMOylation where the upper and lowermost SUMOylated bands disappear. Jra^{K214R} and Jra^{K218R} do not show any loss of bands and behave like the wildtype. Anti-GST western blot (lower panel) post PD showing equal expression of different variants of GST-Jra. The lanes expressing the SUMO(⊗GG) variant serve as a negative control for SUMO conjugation.

E. Anti-His western blot (upper panel) post PD showing the SUMOylated bands of Jra and its mutant variants. Jra^{K29R} shows partial loss of SUMOylation where the two bands on the top disappear. Jra^{K233R}, Jra^{K239R} and Jra^{K248R} do not show loss of higher molecular weight SUMO bands. Anti-GST western blot (lower panel) post PD showing expression of different variants of GST-Jra. The lanes expressing the SUMO-⊗GG variant serve as a negative control for SUMO conjugation.

F. Anti-His western blot (upper panel) of Jra post PD showing the three distinct SUMOylated Jra bands in Jra^{WT}. Partial loss of SUMOylation in Jra^{K29R} and $Jra^{K190R,}$ as seen in panels D and E, is confirmed. $Jra^{K29R+K190R}$ shows complete loss of SUMOylation. Anti-GST western blot (lower panel) post PD showing expression levels of unmodified Jra.

G. *In-vivo* demonstration of SUMOylation of Jra post-Ni-NTA affinity pull-down. Anti-Flag western blot in the upper panel represents the SUMOylated species of Jra and was seen as two distinct bands, marked by asterisks (*). Jra^{K190R} shows loss of the upper band, indicating partial loss of SUMOylation. Jra^{K29R} and $Jra^{K29R+K190R}$ show complete loss of SUMOylation. Jra^{K218R} that was previously shown not to alter SUMOylation status in the bacterial assay, is at par with Jra^{WT}. The empty vector was used as a master negative control. Anti-His western blot (lower panel) represents unmodified Jra and serves as input post affinity PD.

Based on the molecular weight of the SUMOylated species in the Jra^{K29R} and Jra^{K190R} lanes, we suspect that there is a third SUMO site in Jra which is dependent on SUMOylation of Jra^{K29}. However, this third site is not populated either in the Jra^{K29R} single mutant or the $Jra^{K29R+K190R}$ double mutant. Another possibility, di-SUMOylation at Jra^{K29R}, exists, but there is evidence against poly-SUMOylation in insects (Urena *et al.* 2016).

The $Jra^{K29R+K190R}$ is our putative SCR mutant (Jra^{SCR}). To confirm the resistance of this mutant to SUMO conjugation *in-vivo*, we cloned Jra^{WT}, Jra^{K29R}, Jra^{K190R} and $Jra^{K29R+K190R}$ with a 6XHis tag into an inducible pRM vector and transfected 529SU cells transiently with these constructs. 529SU is a stable S2 cell line (Bhaskar *et al.* 2002) that expresses FLAG-SUMO-GG, SAE1, SAE2 and Ubc9 using inducible metallothionein promoters. Expression of Jra variants was initiated by adding CuSO4, which activates the metallothionein promoter. We have performed Ni-NTA affinity pulldown under denaturing conditions, followed by western blots probed with an anti-FLAG antibody and an anti-6XHis antibody (Fig. 1F). In S2 cells, Jra^{WT} showed two SUMO-conjugated bands, corresponding to 1X and 2X SUMOylated species. Jra^{K190R} retained one SUMO conjugation site, but interestingly both Jra^{K29R} and $Jra^{K29R+K190R}$ did

185 not show any SUMO conjugation. Since all further experiments were to be conducted in the
186 animal, and both these sites were high confidence SUMO conjugation sites, we chose to work
187 further with the double mutant, Jra$^{K29R+K190R}$, and defined it as *Jra*^{SCR}.

188 ***Jra and SUMO play critical roles in host defense in the fly gut***

189 After exploring published roles for Jra, we decided to explore Jra function in the gut, which is
190 one of the primary immune organs in the fly (BUCHON *et al.* 2013; MIGUEL-ALIAGA *et al.* 2018).
191 Jra and the other components of the JNK pathway are expressed in various cell types of the
192 gut, with *Jra* upregulated in response to *Pe* infection (DUTTA *et al.* 2015)(Fig. S1). *Jra* transcripts
193 are highest in the enterocytes (ECs, 4.3-fold), followed by the entero-endocrine cells (EEs, 2.7-
194 fold), the interstitial stem cells (ISCs, 1.6-fold) and the enteroblasts (EBs, 1.2-fold) post *Pe*
195 infection (Fig. S1). Flies orally fed with *Pe* rapidly succumb despite the induction of both local
196 and systemic immune responses (VODOVAR *et al.* 2005; LIEHL *et al.* 2006). Hence, we used the
197 *Pe* infection model to study the function of Jra in gut immunity. Since Jra null animals are
198 embryonic lethal, we tested the ability of two well characterised null alleles of *Jra*, *Jra*^{IA109} and
199 *Jra*$^{76-19}$, to resist *Pe* infection in a heterozygous combination with *w*^{1118} (Fig. 2A). Interestingly,
200 the absence of one copy of *Jra* protected the animal against infection, significantly extending
201 lifespan (Fig. 2A). In order to validate this result, we used a gut EC driver, *Myo31DF-Gal4*^{ts}
202 (also called *NP1-Gal4*^{ts}), to reduce Jra function by both RNA interference and by
203 overexpressing a dominant-negative (*Jra*^{DN}) allele. In both experiments (Fig. 2B), reduction of
204 Jra activity in the gut led to partial protection against the pathogen, leading to an extension
205 of lifespan.

206 In contrast, reduction of Jra activity either in the whole animal (Fig. 2A) or in the gut
207 (Fig. 2B) in the absence of infection does not appear to affect lifespan, suggesting that Jra is
208 haplo-sufficient in this context. In flies, the Jra function is activated by a Jun kinase (JNK),
209 Basket (Bsk) (RIESGO-ESCOVAR *et al.* 1996; SLUSS *et al.* 1996). Bsk modulates stem cell
210 proliferation and impacts gut regeneration in *Drosophila* (BITEAU *et al.* 2008; JIANG *et al.* 2009;
211 ZHOU *et al.* 2017). Also, Bsk synergizes with the Imd pathway to regulate epithelial cell
212 shedding during gut infection (ZHAI *et al.* 2018). However, the role of Bsk in the regulation of
213 the gut immune response is not well understood. To test this, Bsk function was attenuated
214 by overexpressing a dominant-negative allele (*Bsk*^{DN}) in the ECs, and the flies were infected
215 with *Pe* (Fig 2C). Interestingly, as in the case of *Jra* knockdown, reduction of Bsk activity also

216 increased lifespan to a similar extent, suggesting that Bsk functions to regulate Jra activation
217 in the host response to infection (Fig. 2C).

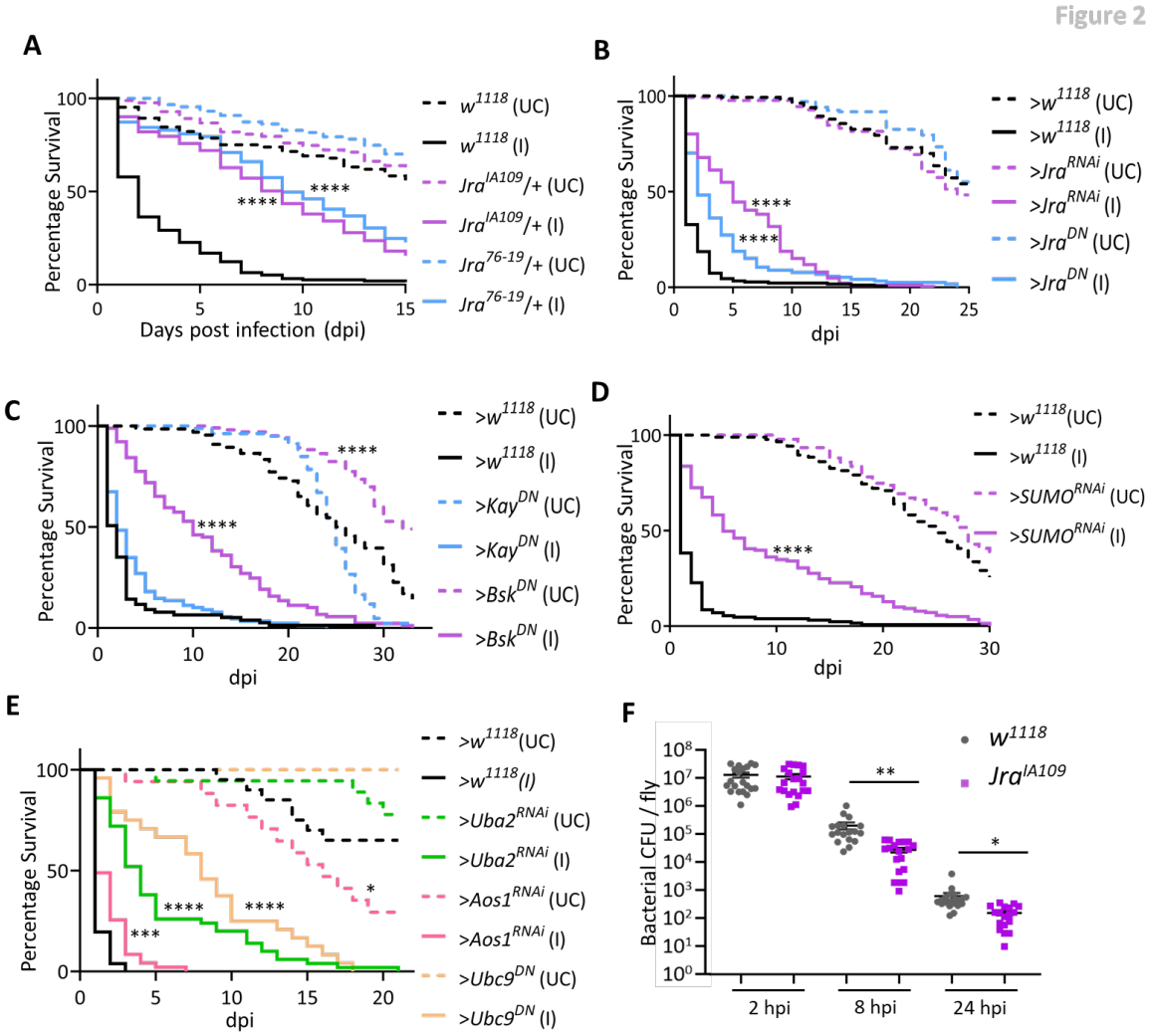

218

219 **Figure 2: Jra signalling and components of SUMO conjugation machinery have important host-defence roles**
220 **in the *Drosophila* gut.**
221 **A.** Survival curves of unchallenged (UC, dotted) and infected (I, closed) flies: w^{1118} (black), Jra^{IA109}/+ (purple) and
222 Jra^{76-19}/+ (blue). Both Jra^{IA109}/+ and Jra^{76-19}/+ flies show enhanced survival upon infection. Log-rank test for trend
223 was used to compare Jra^{IA109}/+ (I) to w^{1118} (I) and Jra^{76-19}/+ (I) to w^{1118} (I). ****p<0.0001.
224 **B.** Survival curves of UC (dotted) and I (closed), flies after over-expression of Jra^{RNAi} (purple) and Jra^{DN} (blue) The
225 *Gal4* control is represented in black. Loss of function of Jra showed enhanced survival upon infection and
226 suggested a gut-specific role of Jra as a suppressor of the immune response. Log-rank test for trend was used to
227 compare >Jra^{RNAi} (I) to >w^{1118} and >Jra^{DN} (I) *to* >w^{1118} (I). ****p<0.0001.
228 **C.** Survival curves of UC (dotted) and I (closed) flies, post-over-expression of Bsk^{DN} (purple) and Kay^{DN} (blue). The
229 *Gal4* control is represented in black. Loss of function of *Bsk* (but not *Kay*) in the gut showed enhanced survival
230 upon infection. Log-rank test for trend was used to compare >Bsk^{DN} (I) to >w^{1118} (I), >Kay^{DN} (I) to >w^{1118} (I) and
231 >Bsk^{DN} (UC) to >w^{1118} (UC). ****p<0.0001.
232 **D.** Survival curves of unchallenged UC (dotted) and I (closed) flies: >w^{1118} (black) and >$SUMO^{RNAi}$ (purple). Loss
233 of SUMO in the gut enhances lifespan post-infection. Log-rank test for trend was used to compare >$SUMO^{RNAi}$ (I)
234 to >w^{1118} (I). ****p<0.0001.

235 **E.** Survival curves of UC (dotted) and I (closed) flies after perturbing different components of the SUMO cycle
236 machinery: >w^{1118} (black), >$Uba2^{RNAi}$ (green), >$Aos1^{RNAi}$ (pink) and >$Ubc9^{DN}$ (orange). Log rank test for trend was
237 used to compare >$Uba2^{RNAi}$ (I) to >w^{1118} (I), >$Aos1^{RNAi}$ (I) to >w^{1118} (I) and >$Ubc9^{DN}$ to >w^{1118} (I) and >Aos^{RNAi} (UC)
238 to > w^{1118} (UC). *p=0.03; ***p=0.0008 ****p<0.0001.
239 **F.** Scatter dot plot representing bacterial load as colony-forming units (CFUs) post-infection. The student's t-test
240 was performed comparing w^{1118} and Jra^{IA109}/+ at respective time points. **p=0.0025; *p=0.0194.
241 *Enterocyte specific NP1-Gal4^{ts} was used to express the transgenes. Data related to the number of animals per*
242 *experiment and replicates listed in Fig. S2A. Data not significant, not represented.*
243

244 Surprisingly, loss of function of Bsk in the gut enhanced lifespan in non-infected
245 conditions. This may suggest that Bsk is a kinase for additional proteins in the gut that regulate
246 the fly's lifespan. Kayak (Kay) can also partner with Jra for transcriptional regulation, with the
247 heterodimeric Jra/Kay complex orthologous to the Jun/Fos AP-1 complex (RIESGO-ESCOVAR AND
248 HAFEN 1997; CIAPPONI AND BOHMANN 2002). In the fly gut, however, reducing the function of Kay
249 did not appreciably change the lifespan of the adult fly (Fig. 2C) post-infection, possibly
250 indicating a Kay-independent role for Jra in responding to *Pe* infection in the gut.
251 Since this study aims to understand the roles of Jra SUMOylation, we also tested the
252 effect of the reduction of global SUMOylation in the gut. Knockdown of *Smt3*/*SUMO* in the
253 gut using *NP1-Gal4^{ts}* was again protective under infective conditions (Fig. 2D). Further,
254 knockdown of the enzymes that contribute to SUMO conjugation, namely *SAE1/Aos1*,
255 *SAE2*/*Uba2*, was also protective, extending adult fly lifespan during *Pe* infection (Fig. 2D), as
256 was the expression of a dominant-negative allele of the conjugating enzyme, *Lwr/Ubc9*
257 (*Ubc9^{DN}*). Under non-infective conditions, loss of SUMO conjugation appeared to affect
258 lifespan, with *Aos1* knockdown reducing lifespan significantly compared to *NP1-Gal4^{ts}> w^{1118}*
259 (Fig. 1E).
260 The protective effect of *Jra* knockdown suggests that the *Pe* may be resistant to
261 clearance by the host-defense response in the presence of *Jra*. We measured the colony-
262 forming units (CFUs) in the gut of adult flies, 2 hours, 8 hours and 24 hours post-infection (hpi,
263 Fig. 2F). The number of CFUs gradually decreased as the infection progressed in w^{1118} and
264 Jra^{IA109}/+. However, there were fewer CFUs in the gut, by order of magnitude, in Jra^{IA109}/+
265 animals, when compared to controls at 8 and 24 hours post-infection, suggesting that absence
266 of Jra signaling in the gut epithelium led to better clearance of gut microbes. Early clearance
267 of the pathogen could also lead to decreased damage of the gut epithelium and a concomitant
268 longer lifespan.

269 Infection with *Pe* damages the gut epithelium, triggering the ISCs to divide asymmetrically
270 to replace the differentiated cells (CHAKRABARTI *et al.* 2012). Immunostaining with an anti-
271 phospho-Histone 3 (pH3) antibody in the gut post-infection allows us to measure the extent
272 of ISC proliferation. For this, w^{1118} and Jra^{IA109}/+ flies were fed with *Pe* for 8 hours and dividing
273 cells per midgut were counted (Fig. S2B). When compared to UC flies, there was a strong
274 induction of mitoses upon infection. The number of dividing cells was similar between w^{1118}
275 (I) and Jra^{IA109}/+ (I), suggesting that Jra might not play a dominant role in regulating the
276 intestinal stem cell proliferation upon an immune challenge in the current context.

277 The reduction of Jra activity during a *Pe* infection appears to be protective to the fly
278 in the context of the gut. Although *Jra* transcripts increase in the gut epithelium in response
279 to *Pe* infection, peaking at 12 hours (next section); Their absence reduces the CFUs and also
280 enhances the survival of flies post-infection. Further, reduction of activity of *Bsk* is also
281 protective, suggesting that Bsk and Jra function in a common Jun kinase (JNK) regulatory
282 pathway in the gut. The gut thus appears to merit a detailed study on the roles for SUMO
283 conjugation of Jra. Our data *prima facie* suggests that Jra acts as an important regulator of
284 the host defense response in the gut epithelium.

285 ***Jra is a major regulator of the transcriptional response to Pe infection***

286 To understand the effect of reduced Jra function in the clearance of *Pe* and extending
287 lifespan in infective conditions, we measured the changes in the midgut transcriptome using
288 3'mRNA sequencing (Fig. S3A and described in Materials and Methods). To start with, we
289 measured the kinetics of activation of *Jra* in the gut during the infection and also the extent
290 of knockdown at each time point using quantitative real-time PCR (qRT-PCR; Fig. 3A). We find
291 that *Jra* levels peak at 12 hpi in our experimental setup. In terms of efficiency of knockdown,
292 the *Jra* levels were reduced by at least 60% during the time course of the infection (Fig. 3A).

293 Next, transcriptomes of the midguts were measured at 4, 12, and 24 hpi for both wild-
294 type and after *Jra* knockdown. Principal component analysis (PCA) was performed to estimate
295 the robustness of the dataset (Fig. S3B). We plotted the first two principal components and
296 observed that the data sets were distinct as the infection progressed and were seen as
297 separate clusters (Fig. S3B). We compared the transcriptional changes in $NP\text{-}Gal4^{ts}$ $>Jra^{RNAi}$
298 ($>Jra^{RNAi}$ here onwards) to $NP\text{-}Gal4^{ts}$ $>w^{1118}$ ($>w^{1118}$ here onwards), without an immune
299 challenge (Unchallenged; UC). Upon knockdown, *Jra* is downregulated by 1.2 times on a log

300 2-fold change (log_2FC scale; Table S1). We also report that 292 genes were differentially
301 expressed with a false discovery rate (FDR) <0.1, amongst which 168 genes were upregulated
302 and 124 genes were downregulated in >*Jra*^{RNAi} as compared to >*w*^{1118} (Fig. 3B and Table S1).
303 The genes including components of immune signalling are putative direct (or indirect)
304 transcriptional targets of Jra. The gut-specific AMPs *Drosomysin-like 2* (*Drsl2*), *Drsl3* and
305 peptidoglycan recognition proteins *PGRP-SC1a* and *PGRP-SC1b* are upregulated (Fig. 3C),
306 suggesting a role for Jra in regulating defense genes even in the absence of infection.

307 Next, we compared the transcriptome of >*w*^{1118} and >*Jra*^{RNAi} in response to infection
308 (I). We normalised data from each infection time point to UC of that genotype and have
309 separated the total genes that were differentially expressed in each pairwise comparison. We
310 then looked at the number of genes differentially expressed at each timepoint in >*w*^{1118} and
311 >*Jra*^{RNAi}. The genes identified ranged from 1000-2000 at each time point. Of note, at 12 hpi,
312 the number of significantly different genes in >*Jra*^{RNAi}, were numerically half of that in >*w*^{1118},
313 indicating a major perturbation in the immune transcriptome (Fig. 3D). We also compared the
314 genes that were common to both the genotypes and genes that were unique to either of the
315 genotypes during infection (FDR<0.1; Fig. S4A). A total of 3505 genes were differentially
316 expressed in both the genotypes, with all timepoints taken together (Table S1). Gene ontology
317 (GO) analysis on all the 3505 genes indicates enrichment of several key GO terms like
318 metabolic process, response to stress, Toll and Imd signalling pathway (Fig. S4B).

319 Fig. 3E categorizes a representative set of genes. Analysing log_2FC values of individual
320 genes (Table S1; Fig. 3E) at the three kinetic time points allows us to understand quantitative
321 differences between the immune response for the two genotypes. At the level of the gene
322 transcripts, the effect appears to be context-specific; most AMPs (Fig. 3E) are upregulated
323 post-infection. In >*Jra*^{RNAi} genes such as *AttA, AttB, DptA, DptB, CecA1, CecA2, Drsl4* show
324 higher log_2FC values and appear to be activated strongly in the earliest time point, i.e 4 hpi,
325 further confirmed by qRT-PCR (Fig. S5A and S5B) for *DiptA* and *AttD*. Log_2FC values for the
326 Imd pathway members, *Relish* (*Rel*), seem to be comparable between both the genotypes.

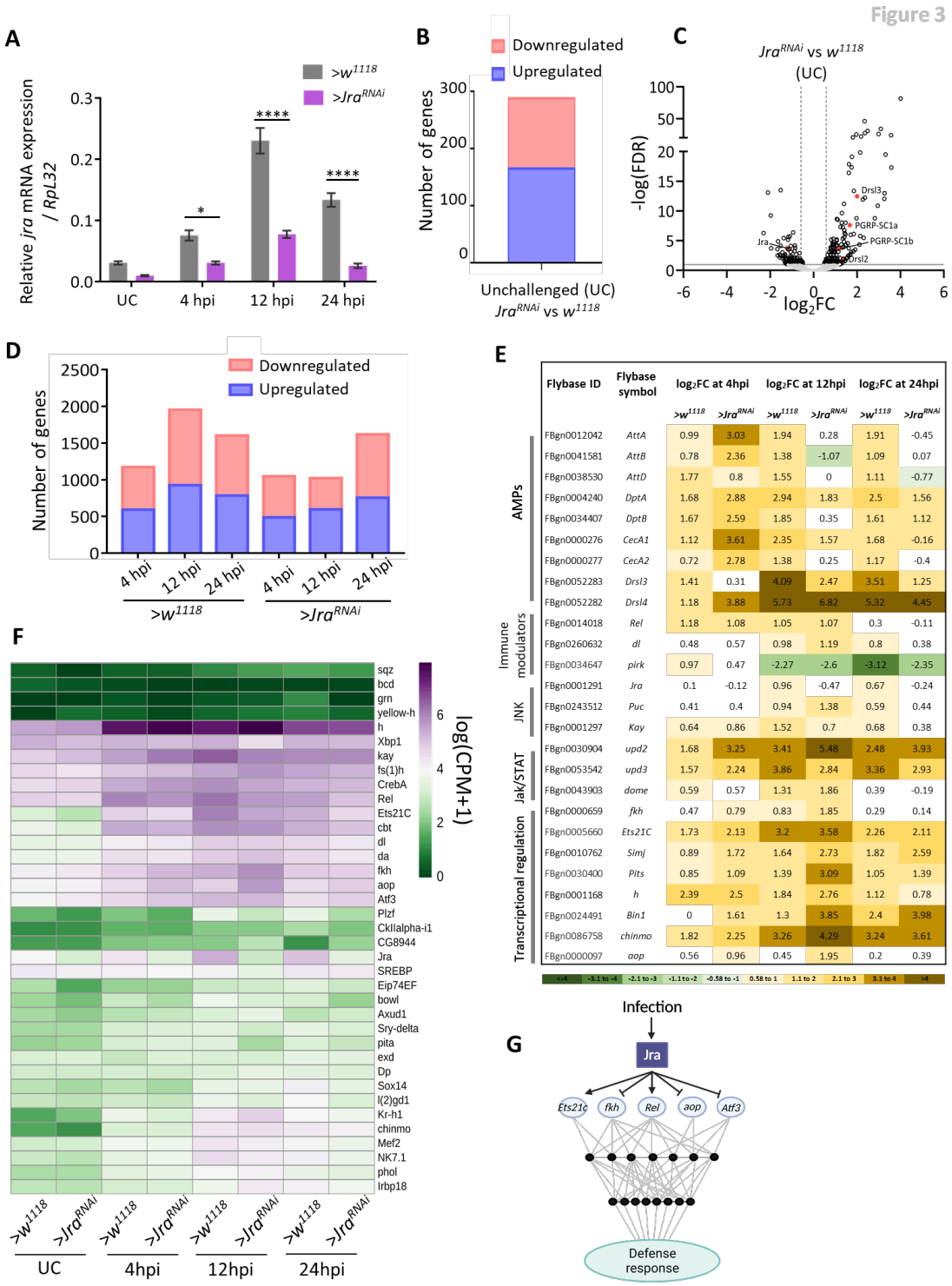

Figure 3: Jra is a major regulator of the *Pe* infected gut transcriptome.

A. Kinetics of activation of Jra transcripts, as measured by qRT-PCR in >w^{1118} and >Jra^{RNAi} without and with gut infection. *p=0.0144, ****p<0.0001 as determined by 2-way ANOVA with Bonferroni's post-hoc test for multiple comparisons. Data from three independent experiments. Means and SEMs represented.

B. Bar plot representation of a total number of significantly differentially expressed genes (FDR<0.1) obtained by comparing >w^{1118} and >Jra^{RNAi} under UC conditions post a 3' mRNA sequencing experiment.

C. Volcano plot showing the up or down-regulated genes, comparing *NP-Gal4*^{ts} >w^{1118} and *NP-Gal4*^{ts} >Jra^{RNAi}. A few genes previously known to function in regulating immunity are highlighted.

D. Bar plot representation of the total number of significantly differentially expressed genes (FDR<0.1) obtained at different hpi after comparing to UC animals of the respective genotype.

E. Tabular representation of log_2FC values of transcripts for a few categories of defence genes regulated during the infection. Log_2FC values in the range 0.58 to -0.58, indicating no significant changes compared to UC, are marked in white.

F. Jra binds to the promoters of several genes (data plotted from modERN dataset ENCSR471GSA). Heatmap represents the normalised expression counts of genes for transcription factors, enriched in the RNA-seq data set, with Jra binding peaks on the promoters.

G. Schematic of Jra immune regulatory network representing the effect of Jra on a subset of transcription factors. The balance between activation and repression of genes by Jra is necessary to evoke a proper and robust immune response.

The same is true for the NFκB transcription factor *dorsal* (*dl*) and members of the JNK pathway, *Puckered* (*Puc)* and *Kay*. However, *poor Imd response upon knock-in* (*Pirk)*, the negative regulator of the Imd pathway (KLEINO *et al.* 2008), had higher log_2FC values in >Jra^{RNAi} compared to w^{1118} at 12hpi. Also, the Jak/STAT pathway components *Upd2* and *Dome* show higher log_2FC values in >Jra^{RNAi} suggesting that the Jak/STAT pathway might be strongly activated in the guts of >Jra^{RNAi} flies. Interestingly, transcriptional regulators like *forkhead* (*fkh)*, *Ets at 21C* (*Ets21C)*, *chronologically inappropriate morphogenesis* (*chinmo)*, *simganj* (*simj)*, *Protein interacting with Ttk69 and Sin3A* (*Pits)*, *hairy (h)*, *Bicoid interacting protein 1*(*Bin1)*, and *anterior open (aop)* show stronger levels of activation in >Jra^{RNAi} throughout the infection. This suggests that Jra could be a major player in a larger gut-specific i-GRN that is activated during an immune response.

Jra can influence the transcription of genes by directly binding to their promoters. We hypothesised that Jra could directly influence the transcription of a subset of the 3505 genes obtained in our experiment. To test this, we used the Jra ChIP-seq dataset available from the modERN consortium (KUDRON *et al.* 2018) and mapped the occupancy of Jra on the promoters of 3505 genes (Fig. S6A, Table S1). We identified a total of 778 genes with enriched peaks of Jra binding on the promoters (Fig. S6A) and considered them as direct transcriptional targets of Jra. We plotted the normalized counts of these 778 genes across all timepoint and two genotypes and observed clear differences in the expression of several genes in >Jra^{RNAi} as compared to >w^{1118} (Fig. S6B). We then performed GO analysis on this subset and confirmed that 'gene-specific transcription' is one of the most represented GO terms (Fig. S6C). Interestingly, there were 37 transcription factors (TFs) in this list, with each transcription factor having the ability to upregulate/downregulate its own set of target genes. Thus the GRN of Jra, along with its target TFs, would define the core Jra-dependent immune gene

372 regulatory network (Jra i-GRN). Hence, we had a closer look at the expression patterns of
373 these TFs (Fig. 3F). Of the 37 TFs, a subset of them responds strongly to infection. These
374 include *h*, *kay*, *Cyclic-AMP response element-binding protein A* (*CrebA)*, *Rel*, *Ets21C*, *cabut*
375 (*cbt)*, dorsal (*dl)*, daughterless (*da)*, *fkh*, *aop*, *Activating transcription factor 3* (*Atf3)*, *Kruppel*
376 *homolog 1* (*Kr-h1)*, *chinmo*, *Myocyte enhancer factor 2* (*Mef2)*, *NK7.1*, and *Jra*. Reduction in
377 *Jra* affected *Rel, Ets21c, Promyelocytic leukaemia zinc finger (Plzf)*, and *brother of odd with*
378 *entrails limited (bowl)* consistently in all the time points and can be seen as reduced levels of
379 transcripts suggesting positive regulation by Jra. Genes like *h*, *fkh*, *aop*, *atf3* and *CG8944* show
380 increased transcript levels upon knockdown of Jra, suggesting negative regulation by Jra.

381 Our data from the transcriptome analysis suggests that loss of Jra in the gut both
382 enhances and suppresses a set of genes (Fig. 3G). The kinetics of upregulation of the AMPs in
383 >Jra^{RNAi} appears to be faster than >w^{1118}, and this could lead to early clearance of bacteria and
384 thus increase the longevity of the infected animal. The Jra i-GRN appears to contain several
385 key transcriptional factors with known gut-specific roles in maintaining homeostasis. These,
386 among several others, include Rel, Ets21C, fkh, aop, and atf3, which are also confident targets
387 of Jra. The influence of Jra on the transcription of these factors could be part of a larger
388 network that is required to activate and suppress genes to evoke a robust immune response
389 (Fig. 3G). Physiologically, the integrated result of the reduction of Jra function and subsequent
390 kinetic modulation of the i-GRN appears to strengthen the host defences, to delay the final
391 victory of the pathogen.

392 ***Generation of Jra^{SCR} by CRISPR/Cas9 genome editing***

393 Having established the functional landscape of Jra function in the gut, we focused on
394 understanding specific roles for SUMO conjugation of Jra. For this, we generated a Jra SCR
395 animal using CRISPR/Cas9 technology. This technology has emerged as a powerful tool to edit
396 the genome and generate point mutations within a gene (BASSETT *et al.* 2013; GRATZ *et al.*
397 2013; GRANT *et al.* 2019). A major benefit of the methodology is the directed nature of the
398 process and the absence of modifications distal from the targeted locus, with the expression
399 of the mutant allele driven by the native promoter. Our strategy involved the use of the
400 Scarless system (GRATZ *et al.* 2014), where a mutant *Jra* genomic template was available after
401 double-stranded break by Cas9 for homology dependant repair (HDR). The stages for
402 generating a $Jra^{K29R+K190R}$ were as follows. A guide RNA (gRNA) that targeted the third exon in
403 the *Jra* locus was designed and cloned into the pBFv-U6.2B vector (Fig. 4A). A transgenic line

404 was generated by targeting the integration of this vector into the second chromosomal attP40
405 site by embryonic microinjection (Fig. 4A). The single guide-RNA line (*Jra*^{sg2}) was balanced and
406 validated. The two SCR mutations that we planned to incorporate into the genomic locus of
407 *Jra* were cloned in the pHD-Scarless-DsRed vector ((GRATZ *et al.* 2014); Fig. 4B). In the Scarless
408 vector, the DsRed cassette is flanked by PBac inverted repeats (IR) that target a TTAA site, and
409 the IRs, in turn, are flanked by the homology regions (HR) specific to the genomic region of
410 interest (Fig. 4B). The DsRed is driven specifically in the eye by the P3 promoter and serves as
411 a proxy for the insertion of the entire cassette into the genomic locus. We incorporated the
412 desired K->R mutations in the 3'HR region and assembled two fragments of *Jra* and two vector
413 fragments using Gibson assembly creating the pHD-Scarless-*Jra*^{SCR} vector (Fig. 4B), which was
414 validated by DNA sequencing.
415 pHD-Scarless-*Jra*^{SCR} was injected into 600 embryos expressing Cas9 and *Jra*^{sg2} (Fig. 4C,
416 D). The F1 animals that emerged were balanced with a 2nd chromosome balancer. Lines that
417 were successfully balanced were screened for positive insertions of the pHD-Scarless-*Jra*^{SCR}
418 by the presence of red fluorescence in the eye of the fly. HDR seemed to be efficient, with 82
419 lines showing integration. A small subset (20) of DsRed positive lines were crossed with a
420 transposase line. The intent was to excise the DsRed cassette. The TTAA site that is duplicated
421 upon insertion of the cassette is restored into a single genomic TTAA site leaving no 'scar'. Six
422 out of the 20 lines showed a loss of DsRed fluorescence, and these flies were rebalanced and
423 sequenced. Only two out of the six lines had K->R mutations at both positions (29th and
424 190th), and we have extensively characterised these lines in the further sections. Three lines
425 harboured K->R mutation only on the 29th position and not the 190th position. One line did
426 not harbour any K->R mutations, and this line was used as a CRISPR control for all the further
427 experiments and referred to as *Jra*^{WT} (Fig. 4E). The *Jra* genomic region was sequenced to
428 confirm that no new mutations were generated in the region. All the six lines were
429 homozygous viable, isogenic and lost the balancers in a couple of generations.
430

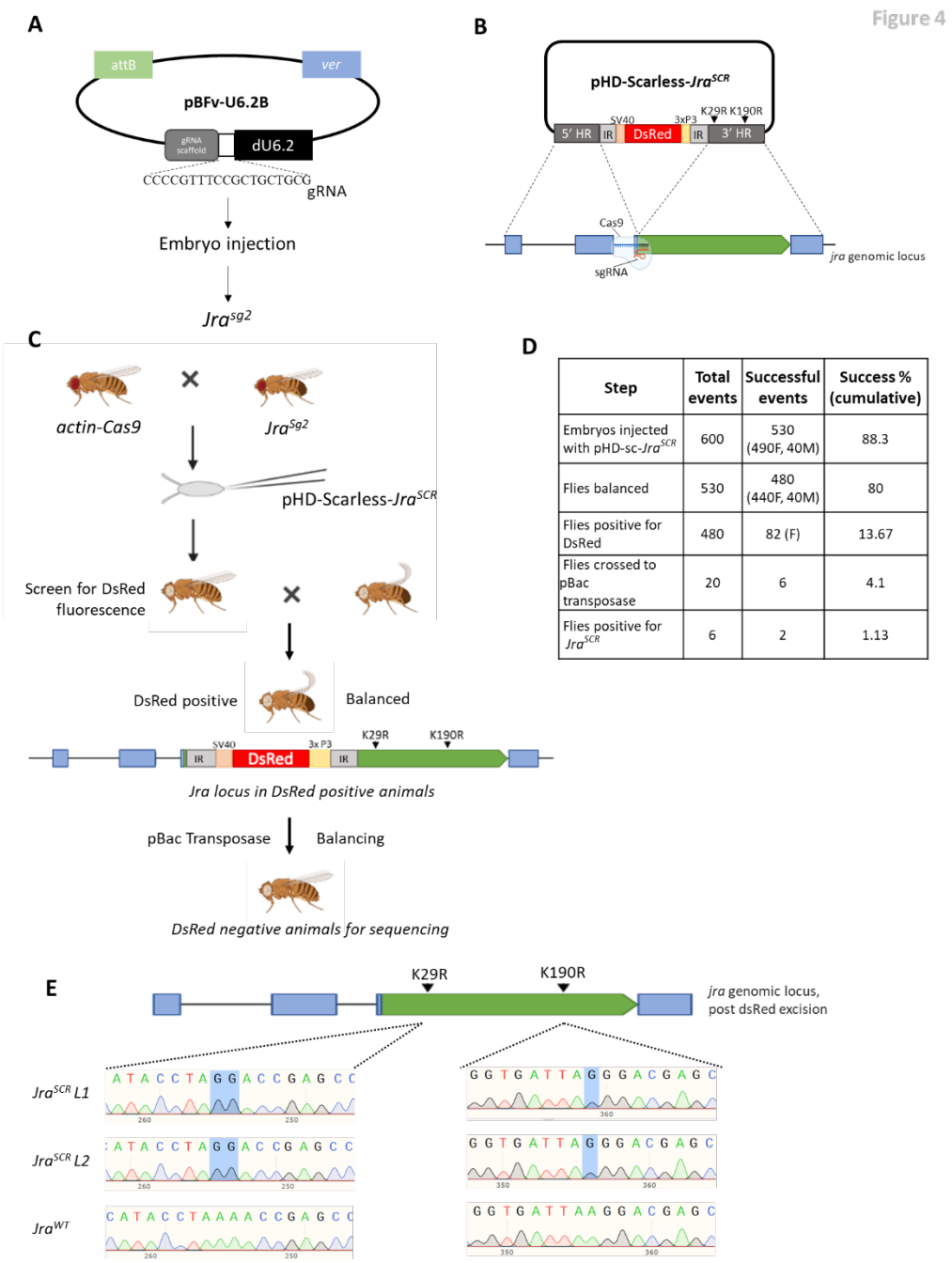

Step	Total events	Successful events	Success % (cumulative)
Embryos injected with pHD-sc-Jra^{SCR}	600	530 (490F, 40M)	88.3
Flies balanced	530	480 (440F, 40M)	80
Flies positive for DsRed	480	82 (F)	13.67
Flies crossed to pBac transposase	20	6	4.1
Flies positive for Jra^{SCR}	6	2	1.13

Figure 4: CRISPR/Cas9 genome editing is used to generate the Jra^{SCR} line.

A. The guide RNA transgenic line, Jra^{sg2}, was created for generating a double-stranded break in the *Jra* locus. A *Jra* locus-specific gRNA fragment (5'CCCCGTTTCCGCTGCTGCG3') was designed and inserted into the pBFV-U6.2B vector.

B. Design and cloning strategy for generating the pHD-scarless-Jra^{SCR} vector. Homology regions (HR, in dark grey) from the *Jra* locus (bottom panel) were cloned into the 5' and 3' arms of the vector as shown in the Schematic. The majority of Jra coding region was part of the 3' arm. As part of the design, the gRNA (panel A) was targeted to the CDS which was a part of the 3rd exon. Details of cloning of the vector are listed in Materials and Methods. The construction of the pHD-Scarless-Jra^{SCR} was validated by sequencing.

C. Schematic of injection of pHD-Scarless-Jra^{SCR} and genetic crosses implemented to mutate the genomic locus of *jra* and generate a Jra^{SCR} transgenic fly using CRISPR/Cas9 technology. *actin-Cas9* flies were crossed with the

444 stable Jra gRNA transgenic fly, *Jra*^{sg2}. The embryos from the cross were injected with pHD-Scarless-*Jra*^{SCR}. Flies
445 that emerged were screened for the presence of fluorescent red eyes. DsRed positive flies, with the pHD-
446 Scarless-*Jra*^{SCR} cassette integrated into the Jra locus, were balanced against the w-;Cyo balancer. SCR mutations
447 would presumably have been incorporated as part of the 3' HR arm. Next, excision of the dsRed cassette was
448 carried out by crossing the flies to a line expressing pBac transposase. Lines in the next generation were screened
449 for loss of DsRed. The lines were balanced, post excision and *Jra* locus sequenced to confirm the loss of DsRed
450 and gain of SCR mutations (panel E).
451 **D.** Tabular representation of the efficiency of CRISPR/Cas9 mediated genome editing of Jra. 600 embryos of the
452 Cas9 and gRNA cross were injected with pHD-Scarless-*Jra*^{SCR}. 530 embryos emerged into adults, of which 490
453 were females, and 40 were males. Only 82 of 490 females had red fluorescence in their eyes. 20 fly lines out of
454 the 82 positives were randomly selected and crossed to flies expressing PBac transposase. 6 flies showed loss of
455 red fluorescence in the eye, and all were sequenced. Only 2 of the 6 lines harboured both the desired lysine to
456 arginine mutations.
457 **G.** Snapshot of the chromatogram of sequences showing K29R and K190R mutations in the genomic locus of Jra.
458 L1 and L2 represent two independent lines of *Jra*^{SCR}, and a third line that did not harbour either of the mutations,
459 was used as wildtype control.
460

461 ***SUMO conjugation of Jra attenuates the suppression of immune response by Jra***

462 Earlier, we have shown that Jra is a major regulator of the gut i-GRN. Mechanistically,
463 Jra directly or indirectly regulates key immune effector genes in the gut of *Drosophila* during
464 infection. A comparison of the gut immune transcriptome between *Jra*^{WT} and *Jra*^{SCR} animals
465 would lead to an understanding of the role of SUMOylation in regulating Jra function (Next
466 Section). Before that, we looked for phenotypical differences in *Jra*^{WT} and *Jra*^{SCR} during an
467 infection to attribute an allelic definition to *Jra*^{SCR}. *Jra*^{SCR} flies fed with *Pe* responded poorly to
468 infection and succumbed early (Fig. 5A). This was true for both lines (L1, L2) that we
469 generated. Interestingly, in terms of survival against infection, *Jra*^{SCR} flies were more sensitive,
470 unlike the *Jra* hypomorph (compare Fig. 2A and Fig. 5A). To define the nature of the SCR allele,
471 we crossed the *Jra*^{WT}, and *Jra*^{SCR} flies to *Jra*^{IA109} and performed lifespan experiments on the
472 heterozygotes. Post feeding with *Pe*, *Jra*^{IA109}/*Jra*^{WT} flies lived longer than homozygous *Jra*^{WT}
473 flies upon infection, consistent with the idea that loss of *Jra* was protective, enhancing the
474 ability of the fly to fight the infection. *Jra*^{IA109}/*Jra*^{SCR} animals also survived longer when
475 compared to homozygous *Jra*^{SCR} flies, but not when compared to *Jra*^{IA109}/Jra^{WT}.

476 To further characterize the allele, we generated overexpression (OE) lines for both
477 *Jra*^{WT} and *Jra*^{SCR}. Wild-type and SCR sequences were cloned into the pUASp-attB vector and
478 UAS- *Jra*^{WT} and UAS-*Jra*^{SCR} lines balanced on the third chromosome. Flies with one copy of
479 *Jra*^{WT} and *Jra*^{SCR} survived better than homozygous *Jra*^{SCR} flies suggesting that a single copy of
480 WT Jra is sufficient to rescue the lethality and restore homeostasis in the gut (Fig. 5C). Also,

481 OE of *Jra*^{WT} in the gut was sufficient to partially rescue the survival seen in *Jra*^{SCR} homozygous
482 flies, while overexpression of Jra^{SCR} in the gut of homozygous *Jra*^{SCR} flies did not show any
483 change in lifespan post-infection (Fig. 5C). Since the rescue with OE of *Jra*^{WT} in the enterocytes
484 was only partial, we used Jra specific *Gal4* (*Jra-Gal4*) and looked at the rescue of *Jra*^{SCR} with
485 OE of *Jra*^{WT}. Similar to what was previously observed, flies with a single copy of *Jra*^{WT} and
486 *Jra*^{SCR} survived better than homozygous *Jra*^{SCR} flies. Interestingly, OE of *Jra*^{WT} with *Jra-Gal4*
487 completely rescued the survival of homozygous *Jra*^{SCR}. OE of *Jra*^{SCR}, however, did not alter the
488 survival of the homozygous *Jra*^{SCR} flies. This suggests that the expression of Jra needs to be
489 tightly regulated to evoke a robust immune response and maintain homeostasis. Also, the
490 role of other organs/tissues in contributing to the expression of Jra cannot be ruled out. Our
491 data rule out *Jra*^{SCR} as a loss of function allele or a dominant-negative allele. Based on the
492 behaviour of the allele and the equivalent data from hypomorphic alleles (Fig. 2A, B), *Jra*^{SCR}
493 appears to be a hypermorphic allele with increased activity of Jra. This would also suggest
494 that SUMO conjugation of Jra could reduce Jra activity, an observation previously reported in
495 the mammalian ortholog, c-Jun (MULLER *et al.* 2000; BOSSIS *et al.* 2005).
496 Next, we tested if the sensitivity of *Jra*^{SCR} flies correlates with the ability of the
497 pathogen to survive in the gut. For this, we performed the bacterial clearance assay on *Jra*^{WT}
498 and *Jra*^{SCR} flies. We observed that *Jra*^{SCR} flies were weaker in their ability to clear *Pe* as there
499 were more CFUs as compared to *Jra*^{WT} at 24 hpi (Fig. 5E). This suggested that the defence
500 factors produced by the gut were weaker in Jra^{SCR} animals. We also tested for the ability of
501 ISCs to proliferate post-infection in *Jra*^{WT} and *Jra*^{SCR} flies. In both cases, pH3^{+} cells increased,
502 indicating a stem cell response, but the response appears to be equal in both genotypes (Fig.
503 S7B). SUMOylation of Jra does not appear to have a role in regulating the division of ISCs
504 during infection.
505 The function of *Jra*^{SCR} is thus distinct from *Jra*^{WT}. Compared to Jra hypomorphs, the
506 effect is contrary, both in terms of lifespan and bacterial clearance. This further agrees with
507 our assertion that *Jra*^{SCR} is a hypermorphic allele. Loss of SUMOylation of Jra increases the
508 activity of Jra and thus reduces the ability of the fly to fight infection.
509
510

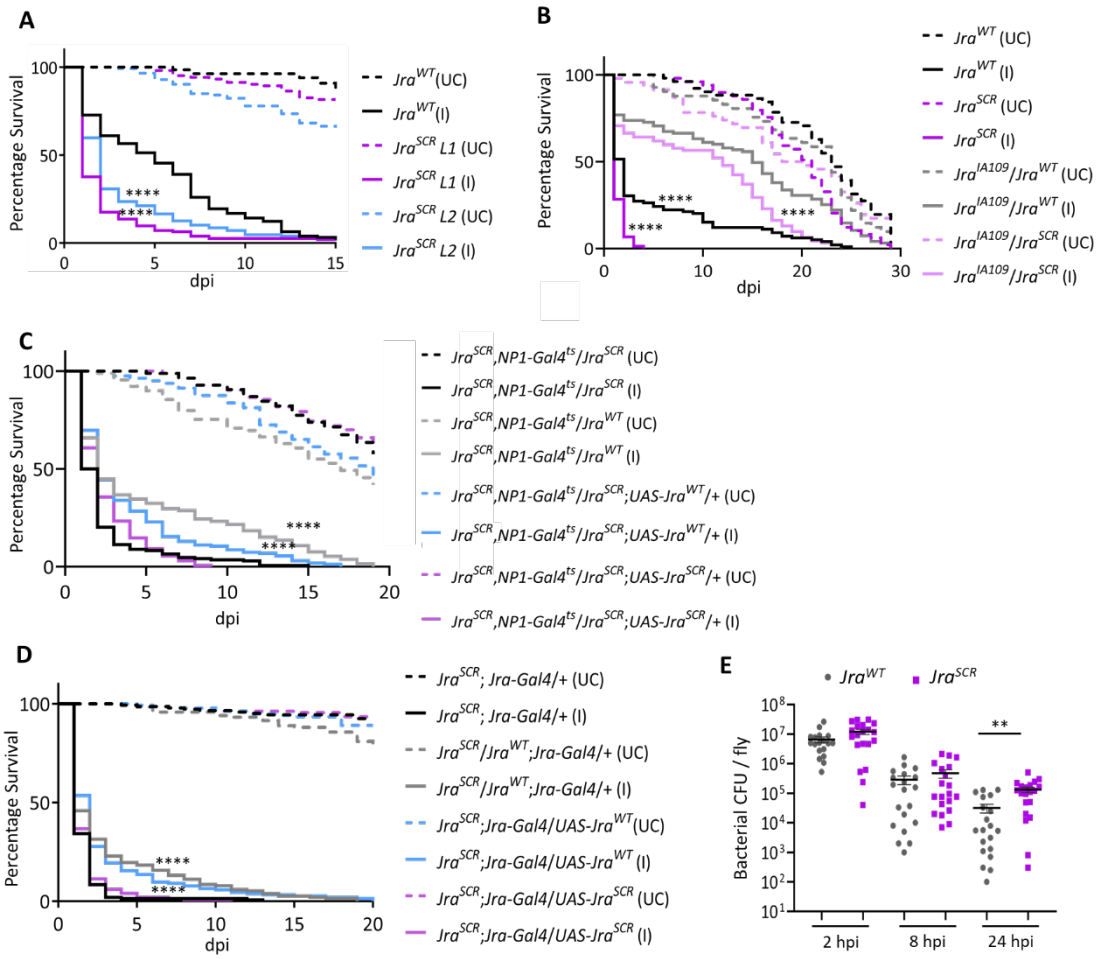

Figure 5: Survival curves post-infection suggest that *Jra^SCR* is a hypermorphic allele

A. Survival curves of unchallenged (UC, dashed lines) and orally infected (I, closed lines), CRISPR/Cas9 modified *Jra^SCR* flies, compared to *Jra^WT*. L1 (red) and L2 (blue) indicate two independent *Jra^SCR* lines used in the experiment. Log-rank test for trend was used to individually compare *Jra^SCR L1* (I) and *Jra^SCR L2* (I) to *Jra^WT* (I). ****p<0.0001.

B. Survival curves of UC (dotted) and I (closed), flies: *Jra^WT* (black), *Jra^SCR* (purple), *Jra^IA109/Jra^WT* (grey) and *Jra^IA109/Jra^SCR* (lavender). Log rank test for trend was used to compare *Jra^IA109/Jra^WT* (I) to Jra^WT (I), *Jra^IA109/Jra^SCR* (I) to *Jra^SCR* (I) and *Jra^IA109/Jra^SCR* (I) to *Jra^IA109/Jra^WT* (I). ****p<0.0001.

C. Survival curves of UC (dotted) and I (closed) flies: *Jra^SCR,NP1-Gal4^ts/Jra^SCR* (black), *Jra^SCR,NP1-Gal4^ts/Jra^WT* (grey), *Jra^SCR,NP1-Gal4^ts/Jra^SCR;UAS-Jra^WT/+* (blue) and *Jra^SCR,NP1-Gal4^ts/Jra^SCR;UAS-Jra^SCR/+* (purple). Log rank test for trend was used to compare *Jra^SCR,NP1-Gal4^ts/Jra^WT* (I), *Jra^SCR,NP1-Gal4^ts/Jra^SCR;UAS-Jra^WT/+* (I) and *Jra^SCR,NP1-Gal4^ts/Jra^SCR;UAS-Jra^SCR/+* to *Jra^SCR,NP1-Gal4^ts/Jra^SCR* (I). ****p<0.0001.

D. Survival curves of UC (dotted) and I (closed) flies: *Jra^SCR;Jra-Gal4/+* (black), *Jra^SCR/Jra^WT;Jra-Gal4/+* (grey), *Jra^SCR;Jra-Gal4/UAS-Jra^WT* (blue) and *Jra^SCR;Jra-Gal4/UAS-Jra^SCR* (purple). Log rank test for trend was used to compare *Jra^SCR/Jra^WT;Jra-Gal4/+* (I), *Jra^SCR;Jra-Gal4/UAS-Jra^WT* (I) and *Jra^SCR;Jra-Gal4/UAS-Jra^SCR* to *Jra^SCR;Jra-Gal4/+* (I). ****p<0.0001.

E. Scatter dot plot representing bacterial load as colony-forming units (CFUs) post oral feeding with *Pe* Student's t-test was performed comparing *Jra^WT* and *Jra^SCR* at respective time point post-infection. **p=0.0015.

Data related to the number of animals per experiment and replicates listed in Fig. S7A. Data not significant is not represented.

532 ***Jra^{SCR} suppresses the activation of defence genes***

533 To gain further mechanistic insight into the role of *Jra^{SCR}*, we have performed a
534 comparative 3'mRNA sequencing experiment with the guts isolated from *Jra^{SCR}* and *Jra^{WT}* at
535 4 and 12 hours post *Pe* infection. PCA indicates that both the genotypes form distinct clusters
536 (Fig. S8A), with the progression of infection. *Jra* levels in *Jra^{WT}* and *Jra^{SCR}* flies were comparable
537 during infection, indicating similar levels of activation (Fig. 6A). Comparing *Jra^{WT}* and *Jra^{SCR}* in
538 UC animals, we find that the transcriptional differences were restricted to a very small
539 number (87; FDR<0.1; Table S2) of genes (Fig. 6B). Genes that are known to regulate immune
540 response were found to be both upregulated, (e.g., *Drosomycin-like 2* (*Drsl2)*, *Attacin-D (AttD)*
541 and *Charon*) and downregulated, (e.g. *Peptidoglycan recognition protein -SC1a* (*PGRP-SC1a)*,
542 *PGRP-SC1b* and *Pirk*), in the *Jra^{SCR}* flies (Fig. 6C). Post *Pe* infection, we identified a total of
543 3134 (FDR<0.1; Table S2) genes to be differentially expressed at 4 hpi and 12 hpi, as
544 normalised to UC in both the genotypes taken together. These genes are plotted in terms of
545 number upregulated downregulated at each time point of the respective genotype (Fig. 6D).
546 We also observed that the changes in genes that were differentially expressed were
547 maximum at 12 hpi (Fig. 6D, Fig. S8B), an observation we previously made (Fig 3) suggesting
548 that major changes in gene regulation occur at 12 hpi in our experimental setup. Gene
549 ontology analysis reveals several key GO terms like metabolic process, gene expression,
550 response to stress, MAPK signalling pathway etc., to be significantly enriched (Fig. S8C) in the
551 genes that are differentially expressed. In order to relate this data to earlier data on Jra loss
552 of function, we evaluated the same set of genes as in Fig. 3E. The $\log_2$FC values of a majority
553 of AMPs (*AttB*, *AttD*, *Cecropin A2* (*CecA2)*, *Diptericin A* (*DptA)*, *Drsl3*, and *Drsl4*) were lower in
554 *Jra^{SCR}* as compared to that of *Jra^{WT}*. The lower levels of AMPs could be one of the reasons for
555 *Jra^{SCR}* flies to succumb early upon infection. Interestingly, the $\log_2$FC values of the
556 transcription factor *Rel* were considerably lower in *Jra^{SCR}* than *Jra^{WT}* in both the infection time
557 points. Also, the $\log_2$FC values of the negative regulator (of the Imd pathway), *Pirk*, appeared
558 to be higher in *Jra^{SCR}* flies than *Jra^{WT}* flies indicating that in *Jra^{SCR}* flies, Imd signalling is
559 dampened. Since Rel is a master immune regulator, we validated this result by performing a
560 quantitative real-time PCR (qRT-PCR) on the guts of *Jra^{WT}* and *Jra^{SCR}* post-infection.

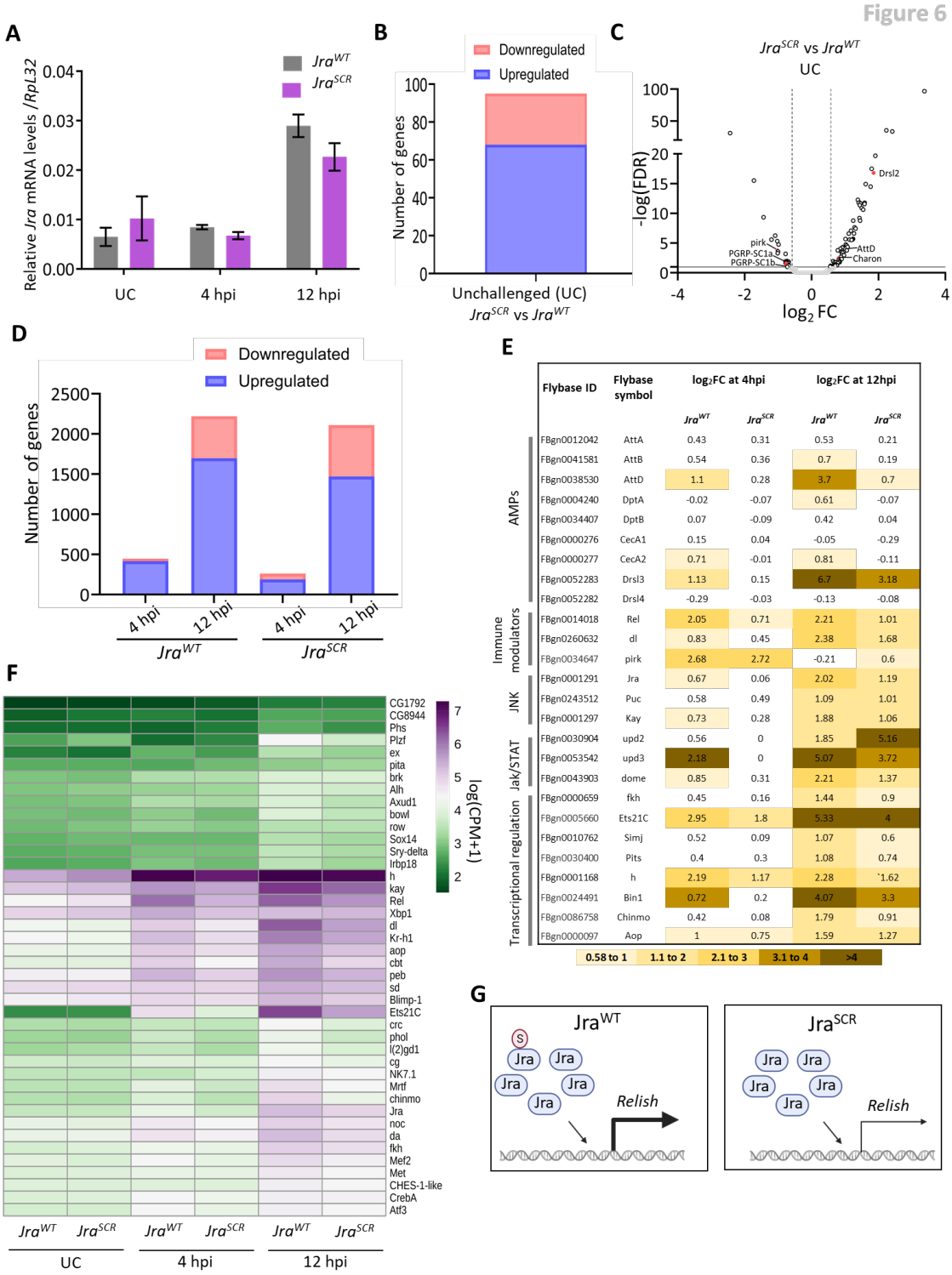

Figure 6: The modulation of the immune response by Jra^{SCR} is distinct from that of Jra^{WT}.

A. Kinetics of activation of Jra transcripts, as measured by qRT-PCR in *Jra^{WT}* and *Jra^{SCR}* without and with gut infection. Data from three independent experiments. Means and SEMs represented.

B. Bar plot representation of a total number of significantly differentially expressed genes (FDR<0.1) obtained by comparing *Jra^{WT}* and *Jra^{SCR}* under UC conditions post a 3' mRNA sequencing experiment.

C. Volcano plot showing the up or down-regulated genes, on comparing *Jra^{WT}* and *Jra^{SCR}*. A few genes previously known to function in regulating immunity are highlighted.

569 **D.** Bar plot representation of the total number of significantly differentially expressed genes (FDR<0.1) obtained
570 at 4 and 12 hpi after comparing to UC animals for the respective genotype.
571 **E.** Tabular representation of log_2FC values of transcripts for a few categories of defence genes regulated during
572 the infection, with a color code at the bottom of the table. Log_2FC values in the range 0.58 to -0.58, indicating
573 no significant changes compared to UC, are marked in white.
574 **F.** Heatmap representing the normalised expression counts of genes for transcription factors, enriched in the
575 RNA-seq data set, with Jra binding peaks on their promoters.
576 **G.** Cartoon representation of the effect of SUMOylation of Jra on *Rel* transcription during infection. In the left
577 panel, Jra^{WT} can be conjugated to SUMO, and this feature helps in the normal activation of *Rel* during the
578 immune response. Whereas, in the case of Jra^{SCR} (right panel), which cannot conjugate to SUMO, *Rel* expression
579 is significantly weaker.
580
581 We found that the activation of *Rel* was suppressed in the guts of Jra^{SCR} (Fig. S9A), the
582 same was true with the activation of *DptA* (Fig. S9B) and *AttD* (Fig. S9C), which are
583 transcriptionally activated by Rel. In contrast, the log_2FC values of components of the JNK
584 pathways were comparable in Jra^{WT} and Jra^{SCR}. A number of transcriptional regulators that
585 showed higher log_2FC values in >Jra^{RNAi} (Fig. 3E) in comparison to w^{1118} showed lower log_2FC
586 values in Jra^{SCR} when compared to Jra^{WT}. Also, the levels of *Upd3* and *Dome* were lower in the
587 Jra^{SCR} flies. Taken together, this suggests that at a molecular level, the genes necessary to
588 negate *Pe* infection are either suppressed or insufficiently activated in Jra^{SCR}, leading to the
589 better survival of the pathogen.
590 As before (Fig. 3), we focused on the genes that could be directly regulated by Jra. For
591 this, we mapped the occupancy of Jra on the 3134 genes differentially expressed, as before.
592 We identified 702 genes with enriched Jra binding peaks on the promoters (Fig. S10A).
593 Plotting the normalised expression of the 702 genes indicated changes between both the
594 genotypes as the infection progressed (Fig. S10B; Table S2) and as previously observed in
595 >w^{1118} and >Jra^{RNAi} dataset, the 'gene-specific transcription' GO term was one of the most
596 represented categories (Fig. S10C). We evaluated gene function and identified 42
597 transcription factors in the list. We plotted the normalised expression counts between the
598 two genotypes during infection to look for changes in the expression pattern of these
599 transcription factors (Fig. 6F). Surprisingly, we observed that the mRNA levels in Jra^{SCR} animals
600 for this subset of genes were lower as compared to Jra^{WT} as the infection progressed. This
601 decrease was considerable in *kay*, *Rel*, *dl*, *aop*, *Kr-h1 cbt* and *Ets21C* at 12 hpi (Fig. 6F) and
602 modest for *h*, *pebbled* (*peb)*, *chinmo*, *Jra*, *da*, *fkh* and *Atf3*.
603 The early lethality seen in Jra^{SCR} flies thus strongly correlates with the findings from
604 the transcriptomics data. We observed that in Jra^{SCR}, several AMPs and key genes that

605 regulate the immune response were insufficiently activated, allowing the pathogen to thrive
606 at the expense of the host. The Jra i-GRN previously described appears to be weakly activated
607 in the *Jra*^{SCR} flies shifting the balance in favor of the pathogen. The mRNA levels of *Rel*, in
608 particular, are significantly lowered in *Jra*^{SCR} (Fig S9), suggesting that SUMOylation of Jra is a
609 necessary event for robust activation of *Rel* in the gut (Fig. 6G).
610

611 **DISCUSSION**

612 The Jun-kinase (JNK) pathway is a well-characterized signalling module used in a wide
613 variety of cellular processes, including, but not limited to proliferation, immunity, apoptosis,
614 and embryonic development. The module is complex with multiple receptors, signalling
615 intermediates, and transcriptional effectors (reviewed by (EFERL AND WAGNER 2003; XIA AND
616 KARIN 2004; DHANASEKARAN AND REDDY 2008; WAGNER AND NEBREDA 2009; ARTHUR AND LEY 2013)).
617 A central theme of the pathway is a cascade of kinases that lead to the activation of a number
618 of the effector transcription factor(s), including c-Jun. In *Drosophila,* the components of the
619 JNK pathway have been well studied (IP AND DAVIS 1998; NOSELLI AND AGNÈS 1999; PEREZ-GARIJO
620 *et al.* 2005; BITEAU *et al.* 2011; RAZZELL *et al.* 2011; RIOS-BARRERA AND RIESGO-ESCOVAR 2013;
621 GALENZA AND FOLEY 2019; BAKER 2020) with Jra also implicated as a transcriptional effector of
622 the systemic immune response in *Drosophila* (KIM *et al.* 2005; KIM *et al.* 2007)(Fig. S11).
623 Current models for the role of Jra in immune signalling for gram-negative infections place it
624 downstream of the PGRP-LC receptor. The pathway bifurcates downstream of Immune
625 Deficient (Imd), with the MAP kinase kinase kinase Tak1 signalling to both Jra and Rel (Fig.
626 S11). The pathway, which is well characterized in flies, involves the IKK complex Kenny/Ird5
627 and leads to phosphorylation and subsequent cleavage of Rel. The N-terminal 68 kD fragment
628 of Rel translocates to the nucleus where it activates the host-defense response. In the parallel
629 path, Tak1 signals to the Jun kinase-kinase Hep, which signals to the JNK Bsk, which in turn
630 activates Jra by phosphorylation (Fig. S11). Jra can function to negatively regulate genes of
631 the host immune response, with a specific example of the AMP *AttA*, where Jra competes
632 with Rel, and shuts off *AttA* transcription (KIM *et al.* 2005; KIM *et al.* 2007). Both Jra and Rel
633 are thus effectors of immune signalling (BOUTROS *et al.* 2002; SILVERMAN *et al.* 2003; KALLIO *et*
634 *al.* 2005; DELANEY *et al.* 2006; BOND AND FOLEY 2009; MYLLYMAKI *et al.* 2014) and there may be
635 considerable overlap between the gene-regulatory networks they activate.
636 Our interest in the functional consequences of SUMO conjugation in the immune response
637 led us to Jra, which is a SUMO target. Also, the role of Jra has not been studied in the context
638 of the gut immune response, making it an exciting candidate to explore. As a first step, we
639 used loss of function Jra alleles, gut-specific Jra knockdowns, and infection with *Pe* to
640 elucidate the role of Jra in regulating the gut immune response. Knockdown of either Jra or
641 Bsk leads to an increase in lifespan post-infection, suggesting that JNK signalling is active in

642 the gut and that pathogen infectivity is facilitated by increased JNK/Jra signalling. Additionally,
643 reduction of global SUMO conjugation in gut ECs was also protective, indicating that the
644 availability of the SUMOylation machinery during infection was helpful to the pathogen. Using
645 gut-specific transcriptomics, we report that the kinetics of activation of AMPs is faster in the
646 guts of the flies with reduced function of Jra, leading to the rapid clearance of bacteria. We
647 have also uncovered a Jra dependent immune gene regulatory network (Jra i-GRN), and this
648 complex network involves several key transcription factors known to maintain gut
649 homeostasis. Examples include Rel (BUCHON *et al.* 2009; BUCHON *et al.* 2014), Fkh (VARMA *et al.*
650 2014; BOLUKBASI *et al.* 2017), Chinmo (GRMAI *et al.* 2018), Ets21C (TOGGWEILER *et al.* 2016;
651 MUNDORF *et al.* 2019), Atf3 (RYNES *et al.* 2012; ZHOU *et al.* 2017), and Aop (ALIC *et al.* 2014; SLACK
652 *et al.* 2015). Jra is required to activate or suppress the transcription of these factors to evoke
653 a robust immune response in the gut against an invading pathogen (Fig. 3G).

654 The Jra SUMO conjugation resistant flies, generated by the CRISPR/Cas9 mediated
655 genome editing, are sensitive to infection and succumb early. One contributory factor to this
656 sensitivity is the persistence of bacteria in the Jra^{SCR} flies, suggesting a weaker host-defense
657 response to the pathogen. In contrast, the loss of Jra function, validated using different
658 hypomorphic alleles, led to a longer lifespan and comparatively fewer bacteria under infective
659 conditions. This would indicate that the Jra-dependent GRN required to evoke a robust
660 immune response in the gut is altered when Jra cannot be SUMOylated. An analysis of the
661 differential gut transcriptional response to the pathogen in Jra^{SCR} and Jra^{WT} animals suggests
662 that the differences lie in the ability of the wild type allele to regulate a subset of defense
663 genes. We propose that the Jra^{SCR} allele is a hypermorph of Jra with increased Jra activity.
664 Interestingly, this increase in activity leads to a lowered and delayed transcriptional response,
665 which gives the pathogen a better foothold and improves its chances for growth and
666 subsequent colonization in the host.

667 One interesting finding is that the NFκB factor *Rel* is insufficiently activated in Jra^{SCR}
668 flies. In addition to this, we have identified other transcription factors of the Jra i-GRN to be
669 either suppressed or insufficiently activated in Jra^{SCR} flies (Fig. 7A). It is important to note that
670 the perturbation of secreted factors such as *upd2* and *upd3* could also influence inter-organ
671 signalling (RAJAN AND PERRIMON 2012; CHAKRABARTI *et al.* 2016), indicating long-range, systemic
672 effects for Jra SUMOylation. We hypothesize that the repression of key transcription factors

673 would influence the transcription of several other genes and compromise the fly's ability to
674 fight infection (Fig. 7A). We propose that SUMOylation of Jra is a crucial step to fine-tune the
675 immune response and maintain homeostasis in the gut of *Drosophila*.
676

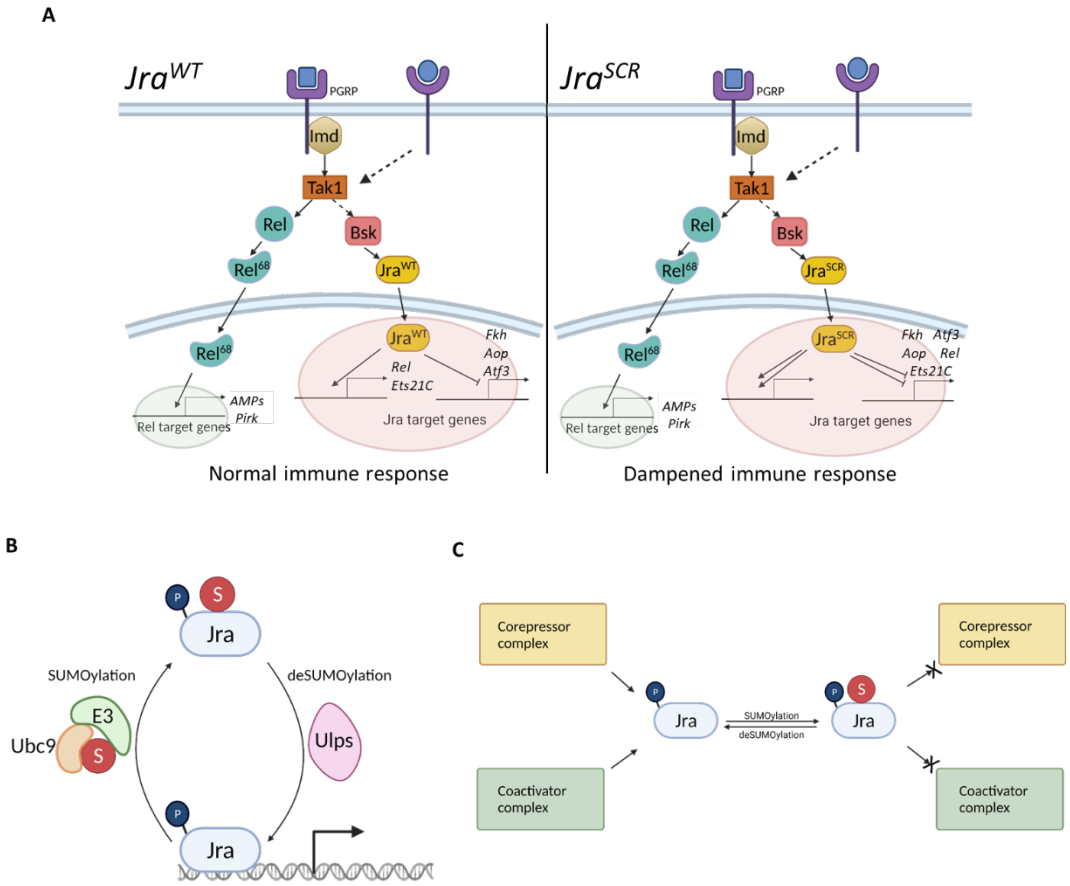

677
678
679 **Figure 7: Regulation of the gut immune response by SUMOylation of Jra**
680 A. The invading pathogen is recognised by the cell surface receptor and the Imd/JNK pathways get activated.
681 Under wildtype conditions where Jra can be SUMOylated (left panel), Jra is required to activate the transcription
682 of *Rel, Ets21C* and repress the transcription of *fkh, aop* and *Atf3.* This is required to evoke a robust immune
683 response and maintain gut immune homeostasis. In a scenario where Jra is resistant to SUMO conjugation, it
684 suppresses the transcription of *Rel* and *Ets21C* along with *fkh*, *aop* and *Atf3*. This leads to insufficient activation
685 of the Jra dependent immune GRN and finally leads to a dampened immune response.
686 B. Dynamics of SUMO conjugation/deconjugation of Jra on the chromatin indicates the fine-tuning of Jra activity
687 by SUMOylation.
688 C. SUMOylation of Jra can alter the interactome of Jra and yield context specific regulation of Jra activity.
689 *Images generated using BioRender.*
690 How does SUMOylation reduce the activity of Jra in the context of transcriptional
691 regulation? Traditionally, Bsk phosphorylates Jra on the N-terminus, leading to the activation
692 of Jra (Sluss *et al.* 1996; Kockel *et al.* 2001), while the mode of deactivation of Jra has been
693 elusive to date. We propose SUMOylation of Jra as a mechanism to attenuate the function of

694 Jra in the context of the gut immune response. We hypothesise that SUMO conjugation/de-
695 conjugation is a dynamic event that happens near the promoters of Jra target genes, and the
696 two states are in equilibrium (Fig. 7B). Depending on the context, there is a shift in this
697 equilibrium, which dictates the outcome of Jra activity. During infection, the transcript levels
698 of Jra rise, leading to an increase in protein levels of Jra. More Jra protein would lead to more
699 active Jra, which could be detrimental to the organism and beneficial to the pathogen. Hence,
700 Jra is SUMOylated to reduce its activity and evoke a potent immune response.

701 One possibility is that SUMOylation of Jra causes Jra to exit the promoter leading to a
702 decrease in overall transcription activity. This argument can be further strengthened by data
703 from the mammalian ortholog, c-Jun, where a SUMO conjugation resistant variant shows
704 higher transcriptional activity (MULLER *et al.* 2000; BOSSIS *et al.* 2005). Consistent with this, the
705 c-Jun binding partner, c-Fos, also shows increased transcriptional activity upon abrogating
706 SUMO conjugation (BOSSIS *et al.* 2005). The SUMOylated form of c-Fos is less abundant on the
707 promoters of select target genes, where SUMOylation knocks c-Fos off the chromatin to
708 disrupt its activity (TEMPE *et al.* 2014). As Jun and Fos are binding partners and perform similar
709 functions, we strongly believe that the same could be happening with SUMOylation of Jra
710 (Fig. 7B). Also, there is evidence that SUMO conjugation negatively regulates the function of
711 a set of transcription factors (BHASKAR *et al.* 2002; MILES *et al.* 2008; OUYANG AND GILL 2009;
712 BOULANGER *et al.* 2021). Another possible mechanism could be a change in interactors,
713 particularly the transcriptional apparatus, that could alter the outcome of Jra activity upon
714 SUMOylation (Fig. 7C). However, we do not rule out the possibility of both these mechanisms
715 acting parallelly in a highly context-specific manner on individual genes.

716 The levels of SUMOylation of any protein at a given time is very low. To test out either
717 of the proposed hypotheses in the current context, one needs to capture the SUMOylated
718 species in abundant amounts in the gut epithelium. With current tools, it becomes challenging
719 to perform ChIP experiments or mass-spectrometry based assays to enrich the SUMOylated
720 species and understand the context-specific role of SUMO conjugation of Jra.

721 In summary, our study establishes Jra's role as a major regulator of the gut immune
722 transcriptome. The Jra and Rel GRN's have substantial overlap with Jra activity regulating
723 defense genes activated by Rel. SUMO conjugation of Jra modulates the immune response,
724 and our study suggests that dampening of the transcriptional regulatory networks is a major
725 feature.

726 MATERIALS AND METHODS

727 Fly husbandry. Flies were reared on standard cornmeal agar at 25°C in a 12-hour light-dark
728 cycle. Only 6-8 day old females were used in all the experiments in this study. All *NP1-Gal4*^{ts}
729 crosses were maintained at 21˚C to inactivate the Gal4. 3 days post eclosion, flies were shifted
730 to 29˚C for 3 days (to activate the Gal4) until bacterial feeding. The flies were shifted to 29°C
731 from the beginning of the infection till the end of the experiment. Table 1 lists the lines used
732 in our studies.

733 Cloning of gRNA and *Jra*^{SCR} for CRISPR/Cas9 mediated genome editing: The gRNA was
734 designed using http://targetfinder.flycrispr.neuro.brown.edu/. The gRNA sequence with no
735 off-targets and optimal for our experimental design was chosen and cloned into the pBFv-
736 U6.2B vector. The 2.5 kb genomic locus of *jra* was amplified from a single *w*^{1118} fly. This was
737 used to generate 3'HR and 5'HR fragments of *jra*. The SCR mutations were incorporated in
738 the 3'HR region. The pHD-scarless-DsRed vector was amplified as two separate fragments
739 using specific primers. The two fragments of *jra* along with the two fragments of the vector
740 were ligated using Gibson assembly (NEB) and sequenced. The 3'HR region cloned into the
741 vector was resistant to the gRNA due to the modification of a few degenerate nucleotides and
742 the PAM sequence. For screening of *Jra*^{SCR} after the excision of DsRed cassette, the genomic
743 DNA was extracted by homogenising single flies in 50ul of a buffer containing 10mM TRIS,
744 1mM EDTA and 20uM Proteinase K. The homogenate was incubated at 37°C for 30 min
745 followed by 85°C for 5 min. 2.5kb of the genomic region of Jra was amplified and sequenced
746 for each line. The *Jra*^{SCR} and *Jra*^{WT} fly lines were regularly sequenced to confirm the desired
747 genotype. All the primers used are listed in table S3.

748

749 **Table 1: Genotypes and source of *Drosophila* lines used for our experiments.**

Line/Genotype	Source	Description
Jra^{WT}	This study	Jra locus modified using CRISPR/Cas9. No mutations incorporated into the genome
Jra^{SCR} *L1*	This study	Jra locus modified using CRISPR/Cas9. K29R+K190R mutations are incorporated into the genome. L1 = line 1. Extensively used in this study
Jra^{SCR} *L2*	This study	Jra locus modified using CRISPR/Cas9. K29R+K190R mutations are incorporated into the genome. L2 = line 2.
Jra^{SCR}*; Jra-Gal4*	This study	*Jra*^{SCR} balanced with *Jra-Gal4*
Jra^{SCR}*,NP1-Gal4*^{ts}*/CyO*	This study	*Jra*^{SCR} recombined with *NP1-Gal4*^{ts}
UAS-Jra^{WT}	This study	pUASp-attB-*Jra*^{WT} inserted into attp40 site

UAS-Jra^{SCR}	This study	pUASp-attB-*Jra^{SCR}* inserted into attp40 site
Jra^{sg2}	This study	gRNA targetting exon 3 of *jra* genomic locus
Jra^{sg2}	This study	gRNA targetting exon 3 of *jra* genomic locus
Myo81F-Gal4, UAS-GFP,tub-gal80^{ts} (NP1-Gal4^{ts})	Sveta Chakrabarti	Enterocyte specific Gal4 line (*NP1-Gal4^{ts}*)
y v[1]; P{y[+t7.7] v[+t1.8]=TRiP.JF01184}attP2	BDSC:31595	*UAS-Jra^{RNAi}*
y[1] w[1118]; P{w[+mC]=Jbz}10	BDSC:7218	*UAS-Jra^{DN}*
w[1118] P{w[+mC]=UAS-bsk.DN}2	BDSC:6409	*UAS-Bsk^{DN}*
w[1118]; P{w[+mC]=UAS-Fra.Fbz}5	BDSC:7214	*UAS-Kay^{DN}*
cn[1] Jra[IA109] bw[1] speck[1]/CyO	BDSC:3273	Jra null
Adh[fn23] pr[1] cn[1] Jra[76-19]/CyO	BDSC:9880	Jra null
y[1] v[1]; P{y[+t7.7] v[+t1.8]=TRiP.HM05055}attP2 /TM3, Sb[1]	BDSC:28569	*UAS-Uba2^{RNAi}*
y[1] v[1]; P{y[+t7.7] v[+t1.8]=TRiP.HM05183}attP2 /TM3, Sb[1]	BDSC:28972	*UAS-Aos1^{RNAi}*
y[1] sc[*] v[1] sev[21]; P{y[+t7.7] v[+t1.8]=TRiP.HMS01540}attP 2	BDSC:36125	*UAS-SUMO^{RNAi}*
UAS-lwr^{DN}	Shubha Govind (HUANG *et al.* 2005)	*UAS-Ubc9^{DN}*
w1118; P{GMR61B05-GAL4}attP2	BDSC:46459	*Jra-Gal4*
y[1] M{Act5C-Cas9.P.RFP-}ZH-2A w[1118] DNAlig4[169]	BDSC:58492	*Actin5c* Cas9
w[1118]	BDSC:3605	*w^{1118}*

Cloning and generation of constructs for overexpression: Jra (FBpp0087498) was amplified from the *Drosophila* gold collection library (https://www.fruitfly.org/EST/gold_collection.shtml) using specific primers (Table S3). These amplicons were independently cloned into the pGEX-4T1 vector for bacterial SUMOylation assay and pRM-HA3 vector for transfection into S2 cells using a modified Seamless Ligation Cloning Extract (SLiCE) protocol (ZHANG *et al.* 2012). The site-directed mutagenesis approach with specific primers was used to modify all the lysine residues to arginine residues to abrogate SUMO conjugation. pUASp-AttB vector was procured from the *Drosophila* Genomics Resource Centre (DGRC, #1358) and was used for targeted insertions of WT/SCR constructs into the attP2 site on the 3rd chromosome. All the clones were confirmed by sequencing and used for downstream experiments.

762 Bacterial SUMOylation assay: This is a modified in-vitro SUMOylation assay that was
763 previously described (NIE *et al.* 2009). The quartet vector comprising of the *Drosophila* SUMO
764 machinery components was co-transformed with GST tagged Jra. The bacterial culture was
765 induced with 1mM of Isopropyl β-D-1-thiogalactopyranoside (IPTG) for 6 hours at 25°C. 10ml
766 of the bacterial culture was harvested in 1ml 50mM *tris* aminomethane (TRIS) buffer
767 containing 150mM NaCl, 1mM Dithiothreitol (DTT), 1ug/ml lysozyme, and 1mM
768 phenylmethylsulfonyl fluoride (PMSF). The cells were lysed using a VibraCell™ probe
769 sonicator with 2/3sec ON/OFF cycle for 2 min at 60% amplitude.
770 S2 cell culture and transfections: S2 cells that were stably transfected with Flag-SUMO
771 (referred to as 529SU cells) were a kind gift from Prof. Albert Courey. The cells were grown
772 and maintained in Gibco® Schneider's *Drosophila* Medium (Thermo Fischer Scientific,
773 #21720024) supplemented with 10% heat-inactivated fetal bovine serum (FBS) (Thermo
774 Fischer Scientific, #10082147) at 23°C. 1ug of plasmid was transfected per 1ml of cells using
775 TransIT®-Insect Transfection Reagent (Mirus, #6100) as per the manufacturer's protocol. The
776 cells were induced with 0.5M CuSO4 and harvested after 48h of induction.
777 Pulldown, Immunoprecipitation and Western blotting**:** Glutathione affinity PD for the
778 bacterial SUMOylation assay was performed using Pierce™ Glutathione Agarose beads
779 (Thermo Fischer Scientific, #16101). Post lysis, the bacterial lysate was incubated with the
780 equilibrated beads for 12-14h at 4°C. The beads were then washed 3 times with the lysis
781 buffer with 0.1% Triton-X100, and bound protein was eluted using 1X laemmli buffer. Ni-NTA
782 superflow resin (Qiagen, #30430) was used to pull down His-Jra from 529SU cells as per the
783 manufacturer's protocol. To maintain stringent denaturing conditions, 8M Urea was used
784 throughout the experiment in all the buffers. 20mM N-ethylmaleimide was also used to
785 inactivate the SENPs. Pierce™ BCA Protein Assay Kit (Thermo Fischer Scientific, #23225) was
786 used to estimate the protein concentration before performing the Western blotting. 1-2mg
787 of total protein for PD and IP experiments and 50ug of total protein for inputs. The following
788 antibodies were used as primary antibodies for the WB. Anti-His (SCBT, #sc-8036; used in
789 1:2000), anti-GST (SCBT, #459; used in 1:5000) and anti-Flag (Sigma-Aldrich, #F7425;used in
790 1:2000). Peroxidase conjugated anti-mouse (Jackson Immunoresearch, #115-035-003; used
791 in 1:10000) and peroxidase-conjugated anti-rabbit (Jackson Immunoresearch, #111-035-003;
792 used in 1:10000) were used as secondary antibodies. All the blots were developed using
793 Immobilon Western Chemiluminescent HRP Substrate (Sigma-Aldrich, #WBKLS). Anti-GST WB

794 and anti-6XHis WB in Fig1 were run on duplicate gels with the same samples. Anti-Flag WB
795 and anti-6XHis WB in Fig 1F were run on duplicate gels with the same samples.
796 Bacterial culture, gut infection, fly survival assays and bacterial clearance assays**:**
797 *Pseudomonas entomophila* (Pe) was used in this study to evoke a robust immune response in
798 the fly gut. The pathogen was always selected for rifampicin (100ug/ml) resistance and
799 hydrolysis of casein on a milk agar plate before the infection experiments. The bacterial pellet
800 obtained from an overnight grown culture was resuspended in a 5% sucrose solution, so the
801 final OD_{600} was ~200. For all the infection experiments, flies were first starved for 2 hours
802 without food and water. Post starvation, the flies were transferred to a fly vial (at 20-30
803 flies/vial) containing Whatman filter disk that was dipped in the concentrated bacterial
804 solution and were allowed to feed for a certain amount of time specific to the experiment.
805 The flies were transferred to a vial containing standard food post-feeding, and the dead flies
806 were counted every 24 hours. Bacterial feeding was carried out for 24 hours for all the survival
807 experiments except when Jra^{SCR} flies were used, where feeding time was 6 hours. For
808 assessing the bacterial load, flies were fed on *Pe* for 2 hours and transferred to vials containing
809 standard food. Before plating, the flies were rinsed in 70% ethanol and left to dry. Whole flies
810 were crushed in sterile PBS, and the lysate was plated on a bacterial agar plate containing
811 rifampicin. The bacterial plates were imaged, and colonies were counted in Fiji (ImageJ) post
812 an intensity cutoff for each plate.
813 Gut dissections, immunostaining and microscopy**:** The guts were precleared by growing the
814 flies on 5% sugar agar overnight for all the immunofluorescence experiments. The next day,
815 flies were fed with *Pe* for 8 hours after 2 hours of starvation. Post feeding, the guts were
816 dissected in ice-cold 1X PBS and fixed in a solution containing 1X PBS, 0.1% TritonX100 and
817 4% paraformaldehyde for 20 minutes. The guts were then incubated at room temperature
818 for an hour in a blocking solution that contained 1X PBS, 0.5% bovine serum albumin, 0.3%
819 TritonX100 and 3% normal goat serum. This was followed by incubation with 1:200 anti-
820 phosphoHistone3 (pH3) antibody (Cell Signalling Technology, #9701L) diluted in blocking
821 solution at 4°C overnight. Anti-rabbit alexa568 (Thermo Fisher Scientific, #A-11011) was used
822 as a secondary antibody in 1:1000 dilution. DAPI was used to mark the nuclei, and the samples
823 were mounted in Slowfade gold antifade mountant (Thermo Fisher Scientific, #36940). The
824 mounted samples were imaged using a 20X oil immersion objective on a Leica SP8 confocal

825 microscope. pH3 positive cells per gut were counted using ImageJ after specifying a threshold
826 and size cutoff (4-20µm^2).
827 qRT-PCR: 1ug of extracted RNA was used to generate cDNA using a high-capacity cDNA
828 reverse transcriptase kit (Thermo Fisher Scientific, #4374966) using the manufacturer's
829 protocol. The cDNA was diluted in a 1:5 ratio for all the experiments. qRT-PCR was performed
830 using gene-specific primers (Table S3) with Kapa SyBr Fast (Sigma-Aldrich, #KK4618) in an
831 Applied Biosystem ViiA 7 real-time PCR system.
832 RNA isolation, 3'mRNA library preparation and sequencing**:** Total RNA was extracted from 50-
833 60 midguts/experiment using RNeasy Plus Universal Kits (Qiagen, #73404) according to the
834 manufacturer's protocol. 3' mRNA specific libraries from three independent biological
835 replicates were amplified using QuantSeq 3' mRNA-Seq Library Prep Kit FWD (Lexogen,
836 #015.96) using the manufacturer's instructions. The concentrations of the libraries were
837 estimated using Qubit™ dsDNA HS Assay Kit (Thermo Fisher Scientific, #Q32851). Quality
838 assessment and library size estimation of the individual libraries was done using an HS DNA
839 kit (Agilent, #5067-4626) in a Bioanalyzer 2100. The libraries were pooled in equimolar ratio,
840 and single-end 75bp reads were sequenced on the Illumina HiSeq 2500 platform.
841 Read mapping, counts generation and differential expression analysis**:** On average, 4-5 million
842 reads were uniquely mapped per sample. Sequencing quality was assessed using FastQC
843 v0.11.5. Post QC, the reads were mapped to the *Drosophila* genome (dm6) using STAR aligner
844 v.2.5.2a (Dobin *et al.* 2013). Gene expression levels were measured using the counts
845 generated by HTSeq-count v 0.6.0 (Anders *et al.* 2015). To obtain differential expression of
846 the genes, the biological conditions were compared pairwise using DESeq2 (Love *et al.* 2014).
847 The above steps were carried out on the bluebee platform
848 (https://lexogen.bluebee.com/quantseq).
849 ChIP-seq data analysis**:** Jra specific ChIP-seq dataset (ENCSR471GSA) against an input dataset
850 (ENCSR908EFA) was obtained from the model organism Encyclopedia of Regulatory Networks
851 (modERN) consortium (https://epic.gs.washington.edu/modERN/) (Kudron *et al.* 2018). Input
852 normalised Bigwig files were used, and the occupancy of Jra was plotted on the gene body
853 (+/- 2kb of the mRNA) of all the significantly differentially expressed genes from the 2 RNA
854 sequencing datasets using deeptools 3.5.0 (Ramirez *et al.* 2016).
855 Bioinformatic analysis: The FDR cutoff < 0.1 was considered for the entire analysis.
856 Normalised counts were generated using the CPM function of edgeR (Robinson *et al.* 2010).

857 The PCA was performed using a custom R script. GO enrichment analysis of the significantly
858 differentially expressed gene set was performed using gProfiler
859 (https://biit.cs.ut.ee/gprofiler/gost) (REIMAND *et al.* 2011) and panther database
860 (http://pantherdb.org/). GO:0003700 'DNA-binding transcription factor activity' term was
861 used to fetch the transcription factors used in the analysis.
862 Statistics: All experiments were performed in three biological replicates unless otherwise
863 specified. Adequate sample size was chosen for each experiment and appropriate statistical
864 test was performed using GraphPad Prism 8.0.
865 Data Deposition: The RNA sequencing data will be deposited in the Gene-Expression Omnibus
866 database on acceptance of the Manuscript.
867
868 **FUNDING**
869 Genome Engineering Technology (GET) grant Department of Biotechnology – Genome
870 Engineering technology grant (BT/PR26095/GET/119/199/2017), Department of
871 Biotechnology (DBT), Govt. of India; Scheme for Transformational and Advanced Research
872 (STARS), Ministry of Education grant 730/2019. The IISER *Drosophila* media and Stock centre
873 is supported by National Facility for Gene Function in Health and Disease (NFGFHD) at IISER
874 Pune, which in turn is supported by an infrastructure grant from the DBT, Govt. of India
875 (BT/INF/22/SP17358/2016). AS was supported by IISER Pune graduate student fellowship and
876 Council of Scientific and Industrial Research (CSIR) – direct SRF fellowship.
877 **CONTRIBUTIONS**
878 AS and GR conceptualized the project and designed the experiments. AS performed all the
879 experiments. AS and GR analysed the data and wrote the manuscript. GR supervised the
880 project and acquired funding.
881 **ACKNOWLEDGEMENTS**
882 We thank: Bloomington *Drosophila* Stock Center (BDSC), Indiana, supported by NIH grant
883 P40OD018537, for fly stocks; Fly facility at the National Centre for Biological Sciences (NCBS),
884 Bangalore for embryonic injections. Dr. Deepti Trivedi for her input on design of the CRISPR
885 Scarless experiments; Dr. Sveta Chakrabarti for providing protocols and reagents related to
886 the infection experiments. Prof. Sanjeev Galande, Dr. Krishnapal Karmodia and Dr. Saurab
887 Pradhan for their inputs on the NGS experiments, reagents and machine time for
888 experiments. Snehal Patil and Yashwant Pawar for fly media and stock maintenance.

889 REFERENCES

890 Adorisio, S., A. Fierabracci, I. Muscari, A. M. Liberati, E. Ayroldi *et al.*, 2017 SUMO proteins:
891 Guardians of immune system. J Autoimmun 84: 21-28.
892 Alic, N., M. E. Giannakou, I. Papatheodorou, M. P. Hoddinott, T. D. Andrews *et al.*, 2014
893 Interplay of dFOXO and two ETS-family transcription factors determines lifespan in
894 Drosophila melanogaster. PLoS Genet 10: e1004619.
895 Anders, S., P. T. Pyl and W. Huber, 2015 HTSeq--a Python framework to work with high-
896 throughput sequencing data. Bioinformatics 31: 166-169.
897 Arthur, J. S., and S. C. Ley, 2013 Mitogen-activated protein kinases in innate immunity. Nat
898 Rev Immunol 13: 679-692.
899 Baker, N. E., 2020 Emerging mechanisms of cell competition. Nat Rev Genet 21: 683-697.
900 Bassett, A. R., C. Tibbit, C. P. Ponting and J. L. Liu, 2013 Highly efficient targeted mutagenesis
901 of Drosophila with the CRISPR/Cas9 system. Cell Rep 4: 220-228.
902 Beauclair, G., A. Bridier-Nahmias, J. F. Zagury, A. Saib and A. Zamborlini, 2015 JASSA: a
903 comprehensive tool for prediction of SUMOylation sites and SIMs. Bioinformatics 31:
904 3483-3491.
905 Bhaskar, V., M. Smith and A. J. Courey, 2002 Conjugation of Smt3 to dorsal may potentiate
906 the Drosophila immune response. Mol Cell Biol 22: 492-504.
907 Biteau, B., C. E. Hochmuth and H. Jasper, 2008 JNK activity in somatic stem cells causes loss
908 of tissue homeostasis in the aging Drosophila gut. Cell Stem Cell 3: 442-455.
909 Biteau, B., J. Karpac, D. Hwangbo and H. Jasper, 2011 Regulation of Drosophila lifespan by
910 JNK signaling. Exp Gerontol 46: 349-354.
911 Bohmann, D., M. C. Ellis, L. M. Staszewski and M. Mlodzik, 1994 Drosophila Jun Mediates
912 Ras-Dependent Photoreceptor Determination. Cell 78: 973-986.
913 Bolukbasi, E., M. Khericha, J. C. Regan, D. K. Ivanov, J. Adcott *et al.*, 2017 Intestinal Fork
914 Head Regulates Nutrient Absorption and Promotes Longevity. Cell Rep 21: 641-653.
915 Bond, D., and E. Foley, 2009 A quantitative RNAi screen for JNK modifiers identifies Pvr as a
916 novel regulator of Drosophila immune signaling. PLoS Pathog 5: e1000655.
917 Bossis, G., C. E. Malnou, R. Farras, E. Andermarcher, R. Hipskind *et al.*, 2005 Down-
918 regulation of c-Fos/c-Jun AP-1 dimer activity by sumoylation. Mol Cell Biol 25: 6964-
919 6979.
920 Boulanger, M., M. Chakraborty, D. Tempe, M. Piechaczyk and G. Bossis, 2021 SUMO and
921 Transcriptional Regulation: The Lessons of Large-Scale Proteomic, Modifomic and
922 Genomic Studies. Molecules 26.
923 Boutros, M., H. Agaisse and N. Perrimon, 2002 Sequential activation of signaling pathways
924 during innate immune responses in Drosophila. Developmental Cell 3: 711-722.
925 Buchon, N., N. A. Broderick and B. Lemaitre, 2013 Gut homeostasis in a microbial world:
926 insights from Drosophila melanogaster. Nat Rev Microbiol 11: 615-626.
927 Buchon, N., N. A. Broderick, M. Poidevin, S. Pradervand and B. Lemaitre, 2009 Drosophila
928 intestinal response to bacterial infection: activation of host defense and stem cell
929 proliferation. Cell Host Microbe 5: 200-211.
930 Buchon, N., N. Silverman and S. Cherry, 2014 Immunity in Drosophila melanogaster--from
931 microbial recognition to whole-organism physiology. Nat Rev Immunol 14: 796-810.
932 Cappadocia, L., and C. D. Lima, 2018 Ubiquitin-like Protein Conjugation: Structures,
933 Chemistry, and Mechanism. Chem Rev 118: 889-918.
934 Celen, A. B., and U. Sahin, 2020 Sumoylation on its 25th anniversary: mechanisms,
935 pathology, and emerging concepts. FEBS J 287: 3110-3140.

936 Chakrabarti, S., J. P. Dudzic, X. Li, E. J. Collas, J. P. Boquete *et al.*, 2016 Remote Control of
937 Intestinal Stem Cell Activity by Haemocytes in Drosophila. PLoS Genet 12**:** e1006089.
938 Chakrabarti, S., P. Liehl, N. Buchon and B. Lemaitre, 2012 Infection-induced host
939 translational blockage inhibits immune responses and epithelial renewal in the
940 Drosophila gut. Cell Host Microbe 12**:** 60-70.
941 Ciapponi, L., and D. Bohmann, 2002 An essential function of AP-1 heterodimers in
942 Drosophila development. Mech Dev 115**:** 35-40.
943 Delaney, J. R., S. Stoven, H. Uvell, K. V. Anderson, Y. Engstrom *et al.*, 2006 Cooperative
944 control of Drosophila immune responses by the JNK and NF-kappaB signaling
945 pathways. EMBO J 25**:** 3068-3077.
946 Dhanasekaran, D. N., and E. P. Reddy, 2008 JNK signaling in apoptosis. Oncogene 27**:** 6245-
947 6251.
948 Dobin, A., C. A. Davis, F. Schlesinger, J. Drenkow, C. Zaleski *et al.*, 2013 STAR: ultrafast
949 universal RNA-seq aligner. Bioinformatics 29**:** 15-21.
950 Dutta, D., A. J. Dobson, P. L. Houtz, C. Glasser, J. Revah *et al.*, 2015 Regional Cell-Specific
951 Transcriptome Mapping Reveals Regulatory Complexity in the Adult Drosophila
952 Midgut. Cell Rep 12**:** 346-358.
953 Eferl, R., and E. F. Wagner, 2003 AP-1: a double-edged sword in tumorigenesis. Nat Rev
954 Cancer 3**:** 859-868.
955 Eifler, K., and A. C. Vertegaal, 2015 Mapping the SUMOylated landscape. FEBS J 282**:** 3669-
956 3680.
957 Flotho, A., and F. Melchior, 2013 Sumoylation: a regulatory protein modification in health
958 and disease. Annu Rev Biochem 82**:** 357-385.
959 Galenza, A., and E. Foley, 2019 Immunometabolism: Insights from the Drosophila model.
960 Dev Comp Immunol 94**:** 22-34.
961 Grant, P. J., A. J. Courey, S. Hanigan, M. S. Kolbe, S. L. Kronick *et al.*, 2019 in *Special Topics in*
962 *Venous Thromboembolism*, Ann Arbor (MI).
963 Gratz, S. J., A. M. Cummings, J. N. Nguyen, D. C. Hamm, L. K. Donohue *et al.*, 2013 Genome
964 engineering of Drosophila with the CRISPR RNA-guided Cas9 nuclease. Genetics 194**:**
965 1029-1035.
966 Gratz, S. J., F. P. Ukken, C. D. Rubinstein, G. Thiede, L. K. Donohue *et al.*, 2014 Highly specific
967 and efficient CRISPR/Cas9-catalyzed homology-directed repair in Drosophila.
968 Genetics 196**:** 961-971.
969 Grmai, L., B. Hudry, I. Miguel-Aliaga and E. A. Bach, 2018 Chinmo prevents transformer
970 alternative splicing to maintain male sex identity. PLoS Genet 14**:** e1007203.
971 Handu, M., B. Kaduskar, R. Ravindranathan, A. Soory, R. Giri *et al.*, 2015 SUMO-Enriched
972 Proteome for Drosophila Innate Immune Response. G3 (Bethesda) 5**:** 2137-2154.
973 Hannoun, Z., G. Maarifi and M. K. Chelbi-Alix, 2016 The implication of SUMO in intrinsic and
974 innate immunity. Cytokine Growth Factor Rev 29**:** 3-16.
975 Hay, R. T., 2005 SUMO: a history of modification. Mol Cell 18**:** 1-12.
976 Hegde, S., A. Soory, B. Kaduskar and G. S. Ratnaparkhi, 2020 SUMO conjugation regulates
977 immune signalling. Fly (Austin) 14**:** 62-79.
978 Hickey, C. M., N. R. Wilson and M. Hochstrasser, 2012 Function and regulation of SUMO
979 proteases. Nat Rev Mol Cell Biol 13**:** 755-766.
980 Huang, L., S. Ohsako and S. Tanda, 2005 The lesswright mutation activates Rel-related
981 proteins, leading to overproduction of larval hemocytes in Drosophila melanogaster.
982 Dev Biol 280**:** 407-420.

983 Ip, Y. T., and R. J. Davis, 1998 Signal transduction by the c-Jun N-terminal kinase (JNK)--from
984 inflammation to development. Curr Opin Cell Biol 10**:** 205-219.
985 Jiang, H., P. H. Patel, A. Kohlmaier, M. O. Grenley, D. G. McEwen *et al.*, 2009
986 Cytokine/Jak/Stat signaling mediates regeneration and homeostasis in the
987 Drosophila midgut. Cell 137**:** 1343-1355.
988 Kallio, J., A. Leinonen, J. Ulvila, S. Valanne, R. A. Ezekowitz *et al.*, 2005 Functional analysis of
989 immune response genes in Drosophila identifies JNK pathway as a regulator of anti-
990 microbial peptide gene expression in S2 cells. Microbes Infect 7**:** 811-819.
991 Kim, L. K., U. Y. Choi, H. S. Cho, J. S. Lee, W.-b. Lee *et al.*, 2007 Down-regulation of NF-κB
992 target genes by the AP-1 and STAT complex during the innate immune response in
993 Drosophila. PLoS Biol 5**:** e238.
994 Kim, T., J. Yoon, H. Cho, W. B. Lee, J. Kim *et al.*, 2005 Downregulation of lipopolysaccharide
995 response in Drosophila by negative crosstalk between the AP1 and NF-kappaB
996 signaling modules. Nat Immunol 6**:** 211-218.
997 Kleino, A., H. Myllymaki, J. Kallio, L. M. Vanha-aho, K. Oksanen *et al.*, 2008 Pirk is a negative
998 regulator of the Drosophila Imd pathway. J Immunol 180**:** 5413-5422.
999 Kockel, L., J. G. Homsy and D. Bohmann, 2001 Drosophila AP-1: lessons from an
1000 invertebrate. Oncogene 20**:** 2347-2364.
1001 Kudron, M. M., A. Victorsen, L. Gevirtzman, L. W. Hillier, W. W. Fisher *et al.*, 2018 The
1002 ModERN Resource: Genome-Wide Binding Profiles for Hundreds of Drosophila and
1003 Caenorhabditis elegans Transcription Factors. Genetics 208**:** 937-949.
1004 La Marca, J. E., and H. E. Richardson, 2020 Two-Faced: Roles of JNK Signalling During
1005 Tumourigenesis in the Drosophila Model. Front Cell Dev Biol 8**:** 42.
1006 Liehl, P., M. Blight, N. Vodovar, F. Boccard and B. Lemaitre, 2006 Prevalence of local immune
1007 response against oral infection in a Drosophila/Pseudomonas infection model. PLoS
1008 Pathog 2**:** e56.
1009 Love, M. I., W. Huber and S. Anders, 2014 Moderated estimation of fold change and
1010 dispersion for RNA-seq data with DESeq2. Genome Biol 15**:** 550.
1011 Melchior, F., 2000 SUMO--nonclassical ubiquitin. Annu Rev Cell Dev Biol 16**:** 591-626.
1012 Miguel-Aliaga, I., H. Jasper and B. Lemaitre, 2018 Anatomy and Physiology of the Digestive
1013 Tract of Drosophila melanogaster. Genetics 210**:** 357-396.
1014 Miles, W. O., E. Jaffray, S. G. Campbell, S. Takeda, L. J. Bayston *et al.*, 2008 Medea
1015 SUMOylation restricts the signaling range of the Dpp morphogen in the Drosophila
1016 embryo. Genes Dev 22**:** 2578-2590.
1017 Mitchell, A. L., T. K. Attwood, P. C. Babbitt, M. Blum, P. Bork *et al.*, 2019 InterPro in 2019:
1018 improving coverage, classification and access to protein sequence annotations.
1019 Nucleic Acids Res 47**:** D351-D360.
1020 Muller, S., M. Berger, F. Lehembre, J. S. Seeler, Y. Haupt *et al.*, 2000 c-Jun and p53 activity is
1021 modulated by SUMO-1 modification. J Biol Chem 275**:** 13321-13329.
1022 Muller, S., C. Hoege, G. Pyrowolakis and S. Jentsch, 2001 SUMO, ubiquitin's mysterious
1023 cousin. Nat Rev Mol Cell Biol 2**:** 202-210.
1024 Mundorf, J., C. D. Donohoe, C. D. McClure, T. D. Southall and M. Uhlirova, 2019 Ets21c
1025 Governs Tissue Renewal, Stress Tolerance, and Aging in the Drosophila Intestine. Cell
1026 Rep 27**:** 3019-3033 e3015.
1027 Myllymaki, H., S. Valanne and M. Ramet, 2014 The Drosophila imd signaling pathway. J
1028 Immunol 192**:** 3455-3462.

1029 Nie, M., Y. Xie, J. A. Loo and A. J. Courey, 2009 Genetic and proteomic evidence for roles of
1030 Drosophila SUMO in cell cycle control, Ras signaling, and early pattern formation.
1031 PLoS One 4: e5905.
1032 Noselli, S., 1998 JNK signaling and morphogenesis in Drosophila. Trends in Genetics 14: 33-
1033 38.
1034 Noselli, S., and F. Agnès, 1999 Roles of the JNK signaling pathway in Drosophila
1035 morphogenesis. Current Opinion in Genetics & Development 9: 466-472.
1036 Ouyang, J., and G. Gill, 2009 SUMO engages multiple corepressors to regulate chromatin
1037 structure and transcription. Epigenetics 4: 440-444.
1038 Perez-Garijo, A., F. A. Martin, G. Struhl and G. Morata, 2005 Dpp signaling and the induction
1039 of neoplastic tumors by caspase-inhibited apoptotic cells in Drosophila. Proc Natl
1040 Acad Sci U S A 102: 17664-17669.
1041 Perkins, K. K., G. M. Dailey and R. Tjian, 1988 Novel Jun-Related and Fos-Related Proteins in
1042 Drosophila Are Functionally Homologous to Enhancer Factor Ap-1. Embo Journal 7:
1043 4265-4273.
1044 Rajan, A., and N. Perrimon, 2012 Drosophila cytokine unpaired 2 regulates physiological
1045 homeostasis by remotely controlling insulin secretion. Cell 151: 123-137.
1046 Ramirez, F., D. P. Ryan, B. Gruning, V. Bhardwaj, F. Kilpert *et al.*, 2016 deepTools2: a next
1047 generation web server for deep-sequencing data analysis. Nucleic Acids Res 44:
1048 W160-165.
1049 Razzell, W., W. Wood and P. Martin, 2011 Swatting flies: modelling wound healing and
1050 inflammation in Drosophila. Dis Model Mech 4: 569-574.
1051 Reimand, J., T. Arak and J. Vilo, 2011 g:Profiler--a web server for functional interpretation of
1052 gene lists (2011 update). Nucleic Acids Res 39: W307-315.
1053 Riesgo-Escovar, J. R., and E. Hafen, 1997 Common and distinct roles of DFos and DJun during
1054 Drosophila development. Science 278: 669-672.
1055 Riesgo-Escovar, J. R., M. Jenni, A. Fritz and E. Hafen, 1996 The Drosophila Jun-N-terminal
1056 kinase is required for cell morphogenesis but not for DJun-dependent cell fate
1057 specification in the eye. Genes Dev 10: 2759-2768.
1058 RiesgoEscovar, J. R., and E. Hafen, 1997 Drosophila Jun kinase regulates expression of
1059 decapentaplegic via the ETS-domain protein Aop and AP-1 transcription factor DJun
1060 during dorsal closure. Genes & Development 11: 1717-1727.
1061 Rios-Barrera, L. D., and J. R. Riesgo-Escovar, 2013 Regulating cell morphogenesis: the
1062 Drosophila Jun N-terminal kinase pathway. Genesis 51: 147-162.
1063 Robinson, M. D., D. J. McCarthy and G. K. Smyth, 2010 edgeR: a Bioconductor package for
1064 differential expression analysis of digital gene expression data. Bioinformatics 26:
1065 139-140.
1066 Rynes, J., C. D. Donohoe, P. Frommolt, S. Brodesser, M. Jindra *et al.*, 2012 Activating
1067 transcription factor 3 regulates immune and metabolic homeostasis. Mol Cell Biol
1068 32: 3949-3962.
1069 Silverman, N., R. Zhou, R. L. Erlich, M. Hunter, E. Bernstein *et al.*, 2003 Immune activation of
1070 NF-kappaB and JNK requires Drosophila TAK1. J Biol Chem 278: 48928-48934.
1071 Slack, C., N. Alic, A. Foley, M. Cabecinha, M. P. Hoddinott *et al.*, 2015 The Ras-Erk-ETS-
1072 Signaling Pathway Is a Drug Target for Longevity. Cell 162: 72-83.
1073 Sluss, H. K., Z. Han, T. Barrett, D. C. Goberdhan, C. Wilson *et al.*, 1996 A JNK signal
1074 transduction pathway that mediates morphogenesis and an immune response in
1075 Drosophila. Genes Dev 10: 2745-2758.

1076 Tempe, D., E. Vives, F. Brockly, H. Brooks, S. De Rossi *et al.*, 2014 SUMOylation of the
1077 inducible (c-Fos:c-Jun)/AP-1 transcription complex occurs on target promoters to
1078 limit transcriptional activation. Oncogene 33**:** 921-927.
1079 Toggweiler, J., M. Willecke and K. Basler, 2016 The transcription factor Ets21C drives tumor
1080 growth by cooperating with AP-1. Sci Rep 6**:** 34725.
1081 Urena, E., L. Pirone, S. Chafino, C. Perez, J. D. Sutherland *et al.*, 2016 Evolution of SUMO
1082 Function and Chain Formation in Insects. Mol Biol Evol 33**:** 568-584.
1083 van der Veen, A. G., and H. L. Ploegh, 2012 Ubiquitin-like proteins. Annu Rev Biochem 81**:**
1084 323-357.
1085 Varma, D., M. H. Bulow, Y. Y. Pesch, G. Loch and M. Hoch, 2014 Forkhead, a new cross
1086 regulator of metabolism and innate immunity downstream of TOR in Drosophila. J
1087 Insect Physiol 69**:** 80-88.
1088 Vierstra, R. D., 2012 The expanding universe of ubiquitin and ubiquitin-like modifiers. Plant
1089 Physiol 160**:** 2-14.
1090 Vodovar, N., M. Vinals, P. Liehl, A. Basset, J. Degrouard *et al.*, 2005 Drosophila host defense
1091 after oral infection by an entomopathogenic Pseudomonas species. Proc Natl Acad
1092 Sci U S A 102**:** 11414-11419.
1093 Wagner, E. F., and A. R. Nebreda, 2009 Signal integration by JNK and p38 MAPK pathways in
1094 cancer development. Nat Rev Cancer 9**:** 537-549.
1095 Xia, Y., and M. Karin, 2004 The control of cell motility and epithelial morphogenesis by Jun
1096 kinases. Trends Cell Biol 14**:** 94-101.
1097 Zhai, Z., J. P. Boquete and B. Lemaitre, 2018 Cell-Specific Imd-NF-kappaB Responses Enable
1098 Simultaneous Antibacterial Immunity and Intestinal Epithelial Cell Shedding upon
1099 Bacterial Infection. Immunity 48**:** 897-910 e897.
1100 Zhang, Y., U. Werling and W. Edelmann, 2012 SLiCE: a novel bacterial cell extract-based DNA
1101 cloning method. Nucleic Acids Res 40**:** e55.
1102 Zhou, J., B. A. Edgar and M. Boutros, 2017 ATF3 acts as a rheostat to control JNK signalling
1103 during intestinal regeneration. Nat Commun 8**:** 14289.
1104

1105

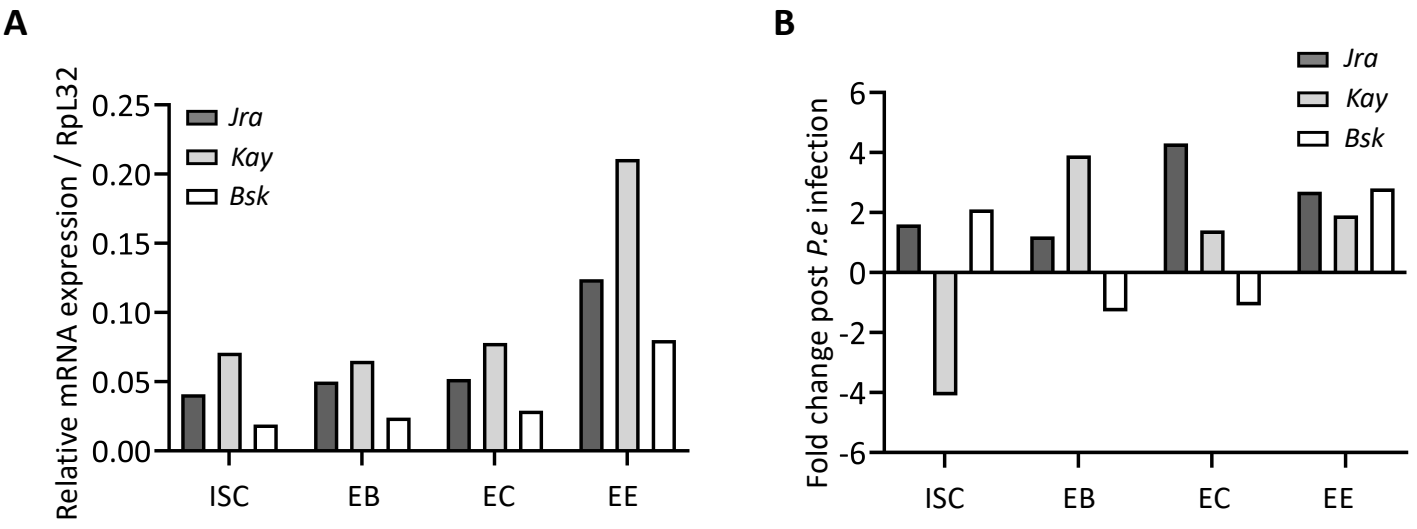

Figure S1: Expression of JNK components in different cell types of the adult gut.

A. Relative mRNA expression of JNK pathway components in different cell types of the adult gut. ISC, Interstitial stem cells; EB, Enteroblast; EC, Enterocytes; EE, Enteroendocrine cells.

B. Fold change of Bsk, Jra and Kay post oral infection with *P.e.*

Both Graphs plotted from data available at http://flygutseq.buchonlab.com/

A

Figure 2	No of Flies used for the experiment	# experiments
A	w^{1118} (UC) – 84; w^{1118} (I) – 154; Jra^{IA109}/+ (UC) – 83; Jra^{IA109}/+ (I) – 161; $Jra^{76\text{-}19}$/+ (UC) – 87; $Jra^{76\text{-}19}$/+ (I) – 141.	3
B	>w^{1118} (C) – 103; >w^{1118} (I) – 141; >Jra^{RNAi} (C) – 91; >Jra^{RNAi} (I) – 141; >Jra^{DN} (C) – 103; >Jra^{DN} (I) – 159.	3
C	>w^{1118} (UC) – 66; >w^{1118} (I) – 77; >Bsk^{DN} (UC) – 79; >Bsk^{DN} (I) – 89 >Kay^{DN} (UC) – 102; >Kay^{DN} (I) – 89.	2
D	>w^{1118} (UC) – 86; >w^{1118} (I) – 128; >$SUMO^{RNAi}$ (UC) – 91; >$SUMO^{RNAi}$ (I) – 141.	3
E	>w^{1118} (C) – 20; >w^{1118} (I) –51; >$Uba2^{RNAi}$ (C) – 18; >$Uba2^{RNAi}$ (I) – 50; >Aos^{RNAi} (C) – 17; >Aos^{RNAi} (I) – 47; >$Ubc9^{DN}$ (C) – 17; >$Ubc9^{DN}$ (I) – 24.	1
F	w^{1118} (2 hpi) – 20; Jra^{IA109}/+ (2 hpi) – 20; w^{1118} (8 hpi) – 17; Jra^{IA109}/+ (8 hpi) – 19; w^{1118} (24 hpi) – 20 ; Jra^{IA109}/+ (24 hpi) – 19.	2

B

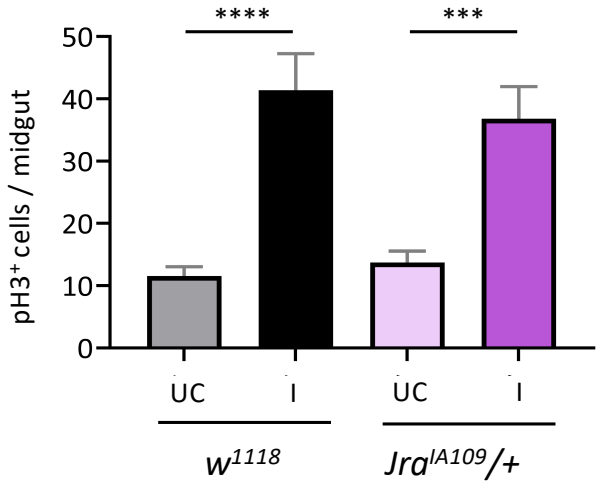

Figure S2: Jra regulates the gut immune response.

A. Tabular representation of the total number of flies used for experiments and number of independent experiments performed in Fig 2.

B. Quantitation of the number of pH3^{+} cells per midgut of UC flies and flies orally fed with *P.e* ****p<0.0001; ***p=0.0011 as determined by 2-way ANOVA with Tukey's post-hoc test. Number of gut used; w^{1118} (UC) – 16; w^{1118} (I) – 17; Jra^{IA109}/+ (UC) – 14; Jra^{IA109}/+ (I) – 17. Means and SEMs represented.

A

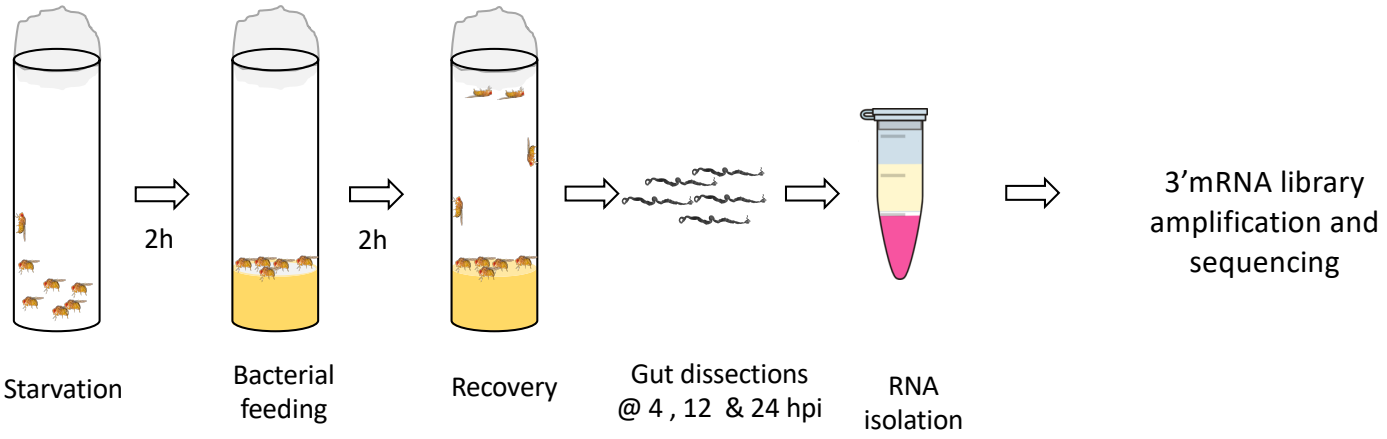

B

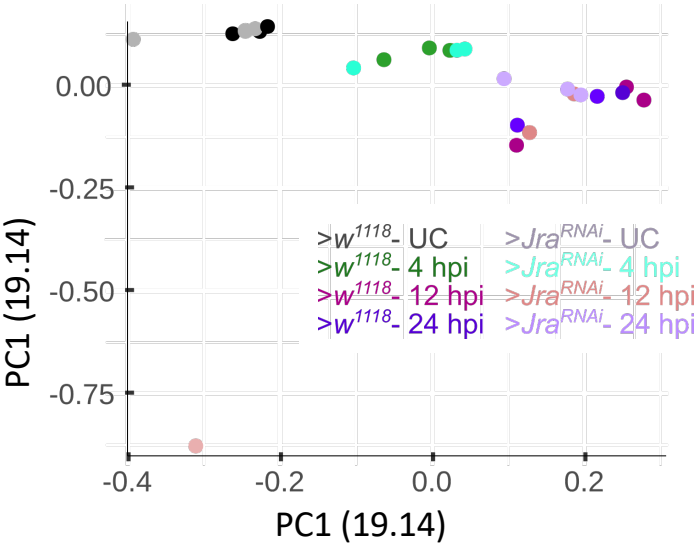

Figure S3: Gut transcriptomics of >*w*^{1118} and >*Jra*^{RNAi}.

A. Schematic of 3' mRNA sequencing experiment. Flies were initially starved (without food and water) for 2h. Flies were then transferred onto a filter paper soaked in concentrated culture of *P.e* and 5% sucrose solution. 2h post feeding, flies were transferred to normal fly food and guts were dissected at 4, 12 and 24 hours post infection (hpi). Gut tissue was homogenized in trizol and RNA was extracted for 3'mRNA sequencing.

B. Principal component analysis (PCA) plot showing the first two principal components of the entire data set.

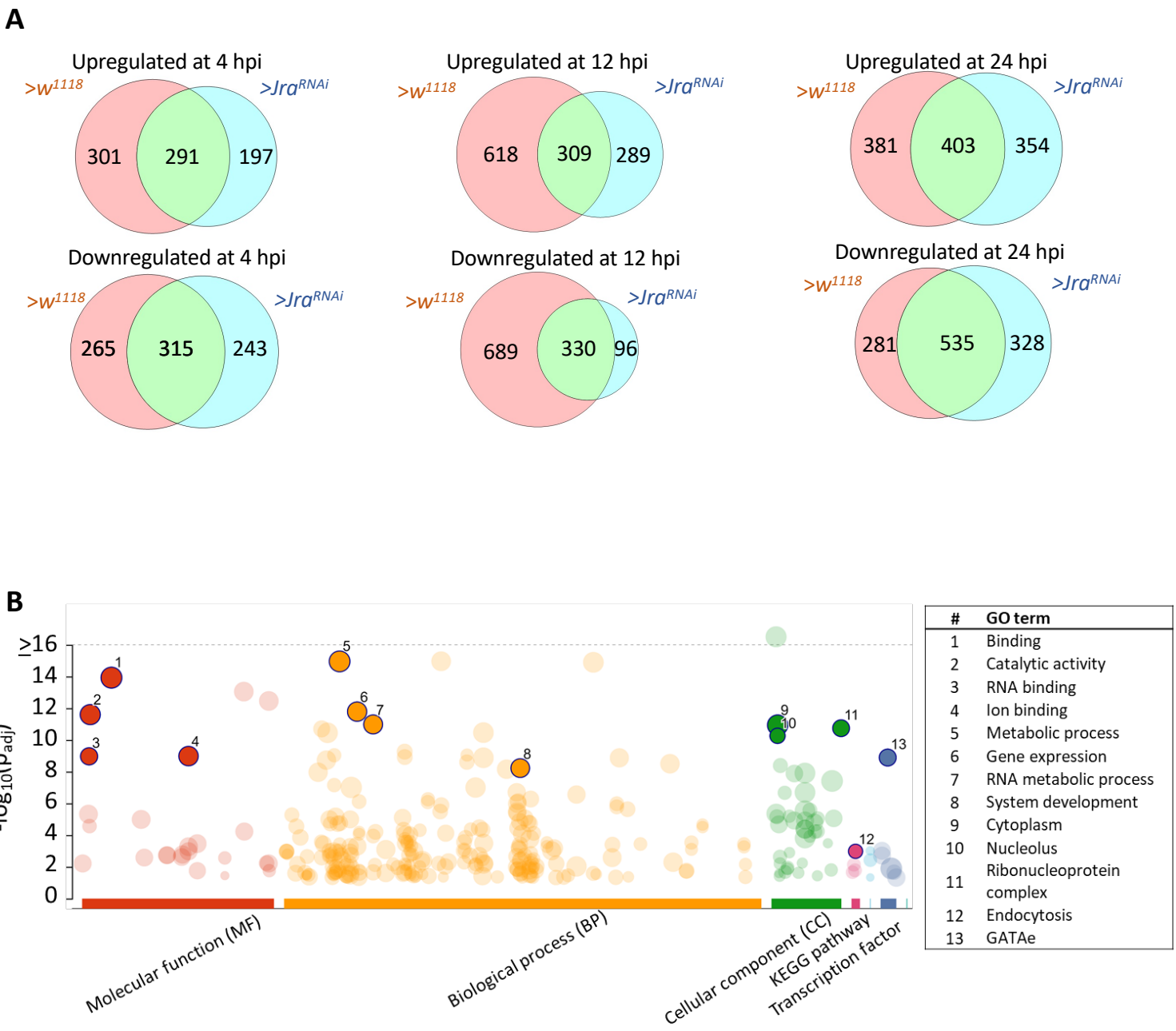

Figure S4: Gut transcriptomics of >*w*^{1118} and >*Jra*^{RNAi}.

A. Venn diagram of significantly differentially expressed genes (FDR<0.1) upregulated and downregulated in >*w*^{1118} and >*Jra*^{RNAi}. The intersection shown in a shade of green represent genes that are significantly differentially expressed in >*w*^{1118} and >*Jra*^{RNAi}.

B. Gene ontology (GO) enrichment analysis of the significantly differentially expressed genes in >*w*^{1118} and >*Jra*^{RNAi} at 4, 12 and 24 hpi. Some key GO terms are highlighted and described

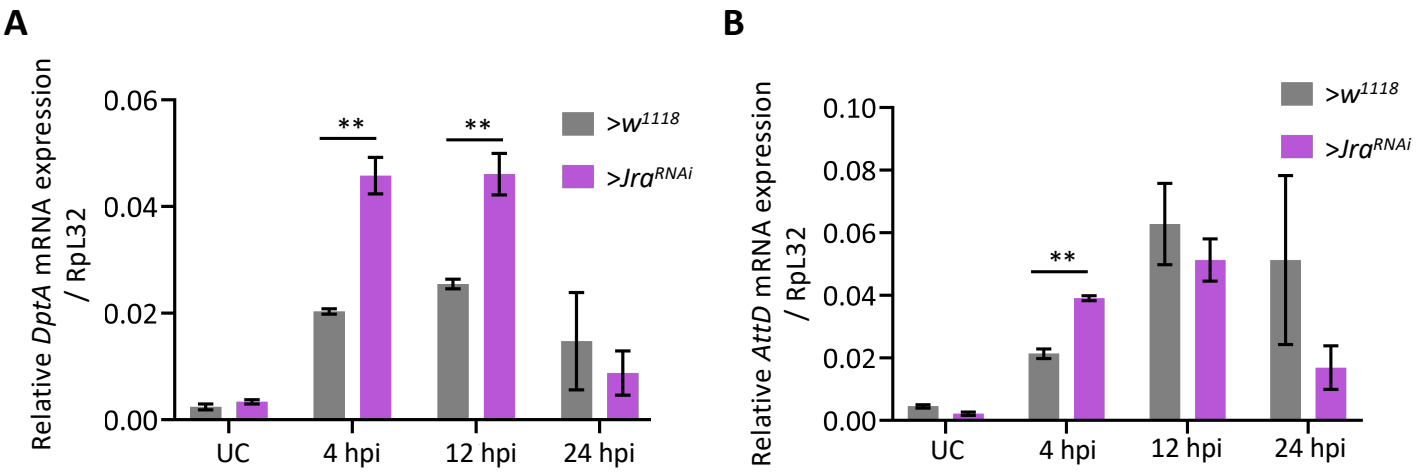

Figure S5: >*Jra*^{RNAi} shows increased expression of AMPs during infection.
qRT-PCR data showing the activation of *DptA* (**A**) and *AttD* (**B**) transcripts during gut infection in >*w*^{1118} and >*Jra*^{RNAi}. **p<0.0091 as determined by 2-way ANOVA with Bonferroni's post-hoc test for multiple comparisons. Data from three independent experiments. Means and SEMs represented.

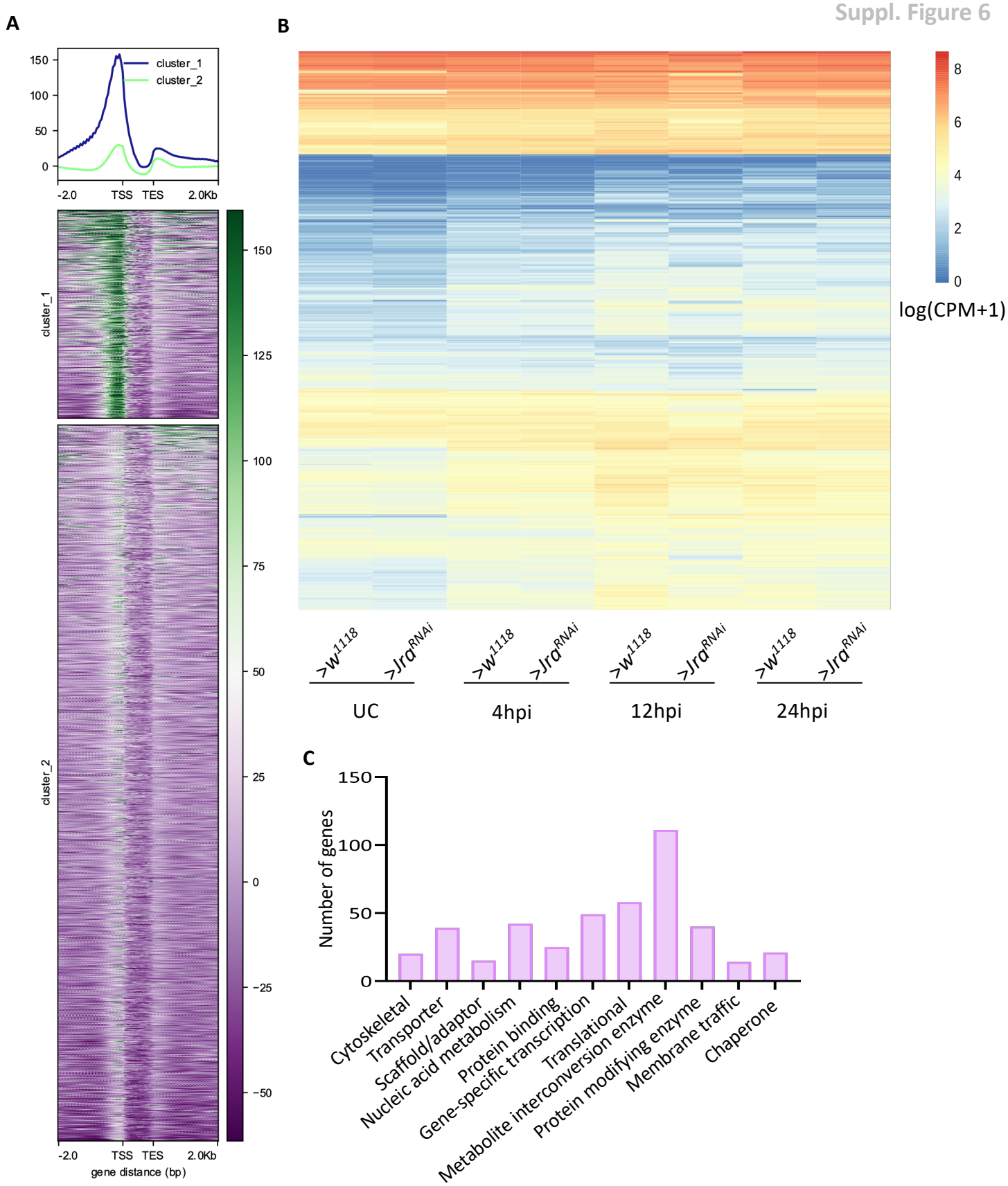

Figure S6: Mapping Jra occupancy on the promoters of differentially expressed genes in >*w*^{1118} and >*Jra*^{RNAi}.

A. Heatmap showing occupancy of Jra on the gene body of the differentially expressed genes in >*w*^{1118} and >Jra^{RNAi}. Cluster 1 represents a set of genes with enriched binding. Heatmap plotted with data extracted from Jra ChIP-seq dataset (ENCSR471GSA) post input (ENCSR908EFA) normalization

B. Heatmap representing the normalised expression counts of genes with enriched Jra (Cluster 1) binding on the promoters.

C. GO terms (Panther-Protein class) of genes with enriched Jra binding on the promoters.

A

Figure 5	No of Flies used in the experiment	# experiments
A	*Jra*^{WT} (UC) – 142; *Jra*^{WT} (I) – 154; *Jra*^{SCR} *L1* (UC) – 103; *Jra*^{SCR} *L1* (I) – 154; *Jra*^{SCR} *L2* (UC) – 111; *Jra*^{SCR} *L2* (I) – 127.	3
B	*Jra*^{WT} (UC) – 51; *Jra*^{WT} (I) – 99; *Jra*^{SCR} (UC) – 49; *Jra*^{SCR} (I) – 74; *Jra*^{IA109}/*Jra*^{WT} (UC) – 41; *Jra*^{IA109}/*Jra*^{WT} (I) – 95; *Jra*^{IA109}/*Jra*^{SCR} (UC) – 46; *Jra*^{IA109}/*Jra*^{SCR} (I) – 92.	2
C	*Jra*^{SCR}, *NP1-Gal4*^{ts}/*Jra*^{SCR} (UC) – 84; *Jra*^{SCR}, *NP1-Gal4*^{ts}/*Jra*^{SCR} (I) – 168; *Jra*^{SCR},*NP1-Gal4*^{ts}/*Jra*^{WT} (UC) – 89; *Jra*^{SCR},*NP1-Gal4*^{ts}/*Jra*^{WT} (I) – 185; *Jra*^{SCR},*NP1-Gal4*^{ts}/*Jra*^{SCR};*UAS-Jra*^{WT}/+ (UC) – 80; *Jra*^{SCR},*NP1-Gal4*^{ts}/*Jra*^{SCR};*UAS-Jra*^{WT}/+ (I) – 162; *Jra*^{SCR},*NP1-Gal4*^{ts}/*Jra*^{SCR};*UAS-Jra*^{SCR}/+ (UC) – 82; *Jra*^{SCR},*NP1-Gal4*^{ts}/*Jra*^{SCR};*UAS-Jra*^{SCR}/+ (I) – 163.	3
D	*Jra*^{SCR};*Jra-Gal4/+* (UC) – 142; *Jra*^{SCR};*Jra-Gal4/+* (I) – 155; *Jra*^{SCR}/*Jra*^{WT};*Jra-Gal4/+* (UC) – 117; *Jra*^{SCR}/*Jra*^{WT};*Jra-Gal4/+* (I) – 153; *Jra*^{SCR};*Jra-Gal4/UAS-Jra*^{WT} (UC) – 136; *Jra*^{SCR};*Jra-Gal4/UAS-Jra*^{WT} (I) – 155; *Jra*^{SCR};*Jra-Gal4/UAS-Jra*^{SCR} (UC) – 132; *Jra*^{SCR};*Jra-Gal4/UAS-Jra*^{SCR} (I) – 150.	3

B

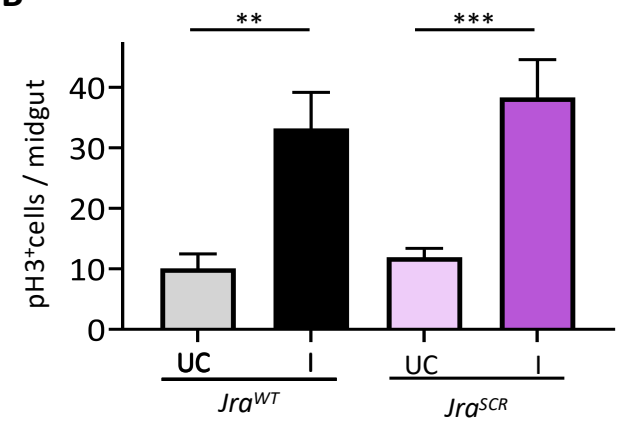

Figure S7: *Jra*^{SCR} dampens the gut immune response.

A. Tabular representation of the total number of flies used for experiments and number of independent experiments performed in Fig 5.

B. Quantitation of number of pH3^{+} cells per midgut of UC flies and flies orally fed with *P.e*. **:p=0.0071; ***p=0.0005 as determined by 2-way ANOVA with Tukey's post-hoc test. Number of gut used; *Jra*^{WT} (UC) – 20; *Jra*^{WT} (I) – 23; *Jra*^{SCR} (UC) – 24; *Jra*^{SCR} (I) – 24. Means and SEMs represented.

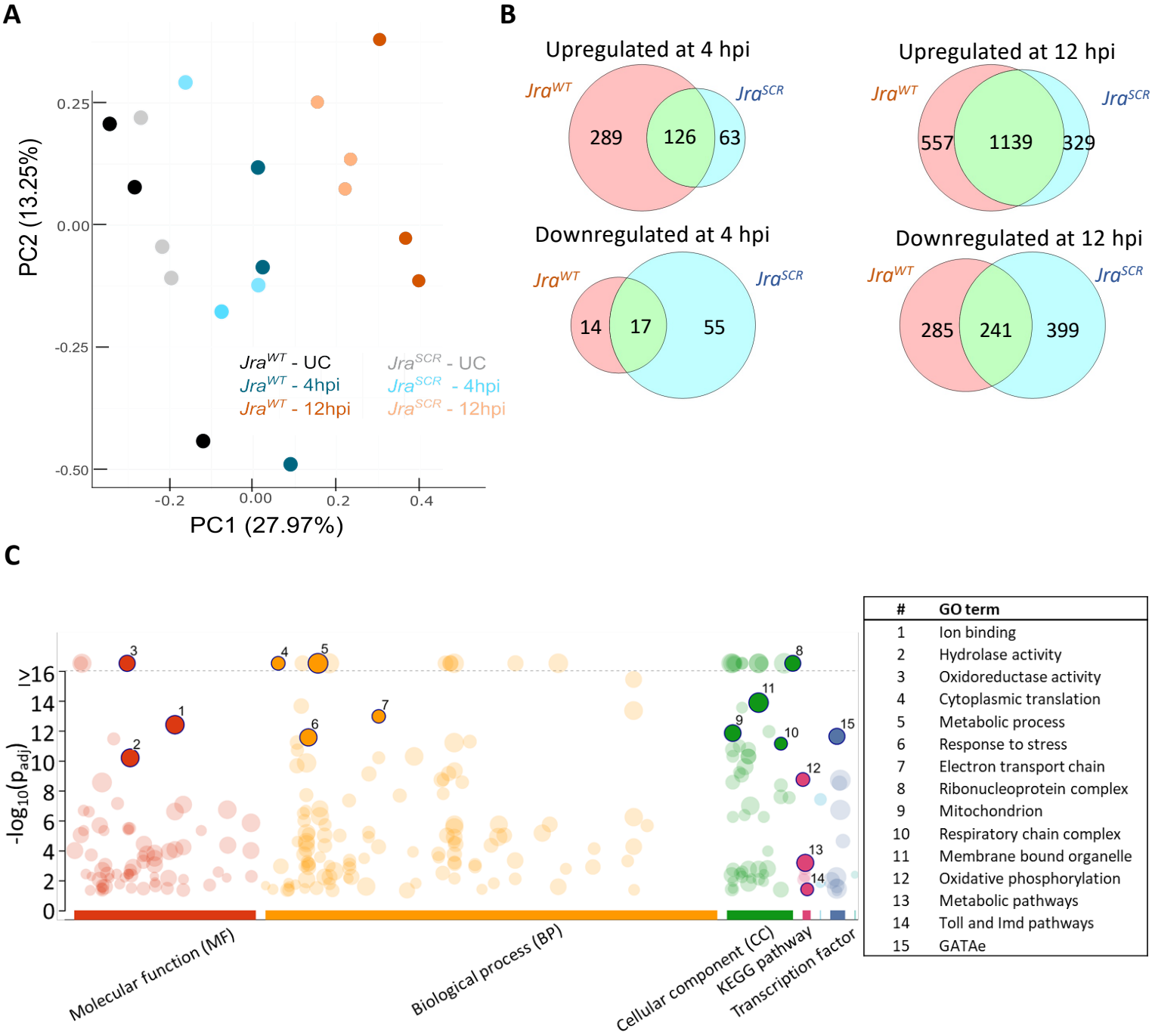

Figure S8: Gut transcriptomics of *Jra^WT* and *Jra^SCR*.

A. Principal component analysis (PCA) plot showing the first two principal components of the entire data set.

B. Venn diagram of significantly differentially expressed genes (FDR<0.1) upregulated and downregulated in *Jra^WT* and *Jra^SCR*. The intersection shown in a shade of green represent genes that are common in *Jra^WT* and *Jra^SCR*.

C. Gene ontology (GO) enrichment analysis of the significantly differentially expressed genes from the entire data set. Some key GO terms are highlighted and described

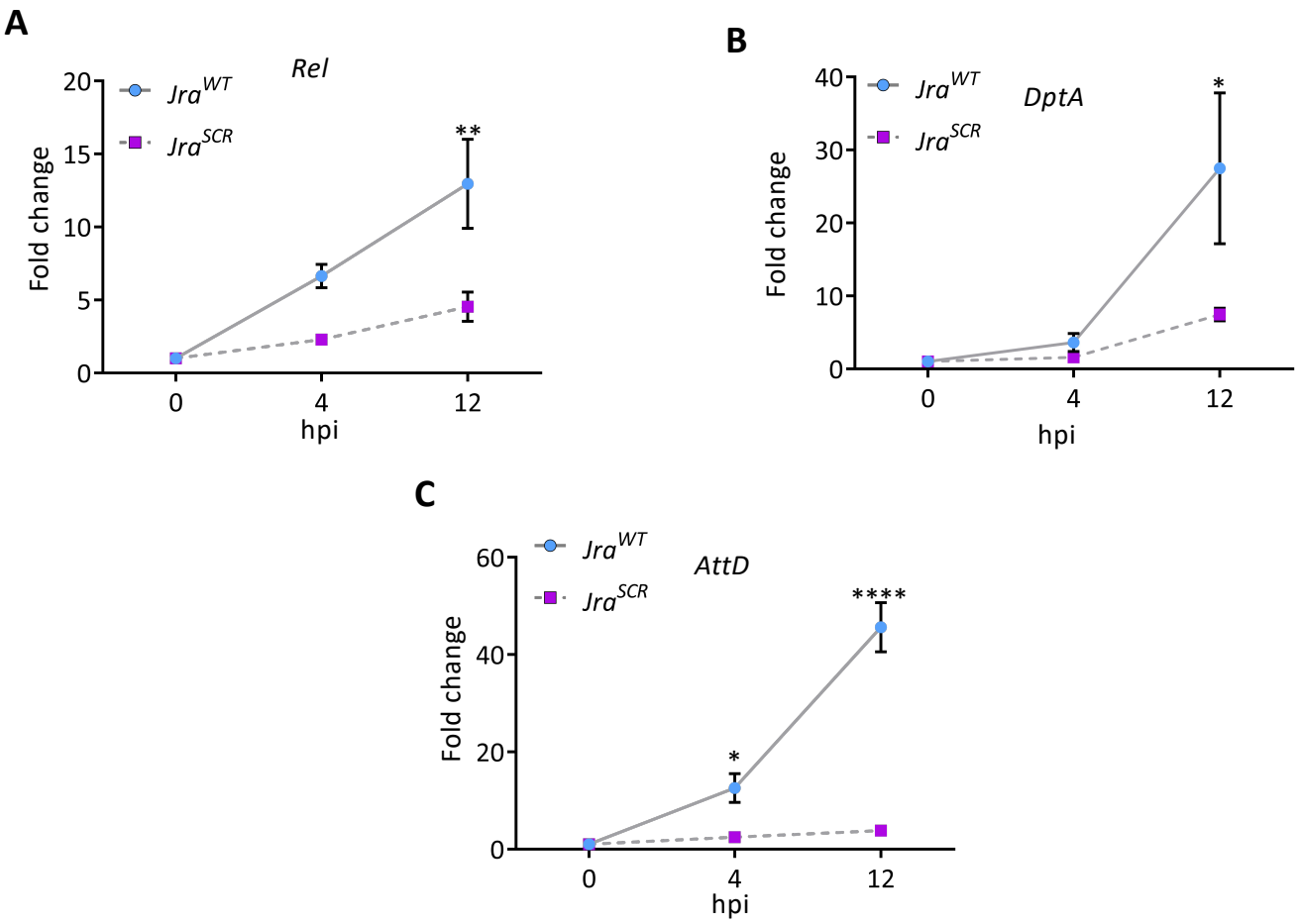

Figure S9: *Jra^SCR* shows insufficient activation of key immune effectors.
qRT-PCR data showing the activation of *Rel* (**A**), *DptA* (**B**) and *AttD* (**C**) transcripts during gut infection in Jra^{WT} and Jra^{SCR}. *p=0.0182 (*DptA*-12hpi), *p=0.0365 (*AttD*-4hpi), **p=0.0027, and ****;p<0.0001 as determined by 2-way ANOVA with Bonferroni's post-hoc test for multiple comparisons. Data from three independent experiments. Means and SEMs represented.

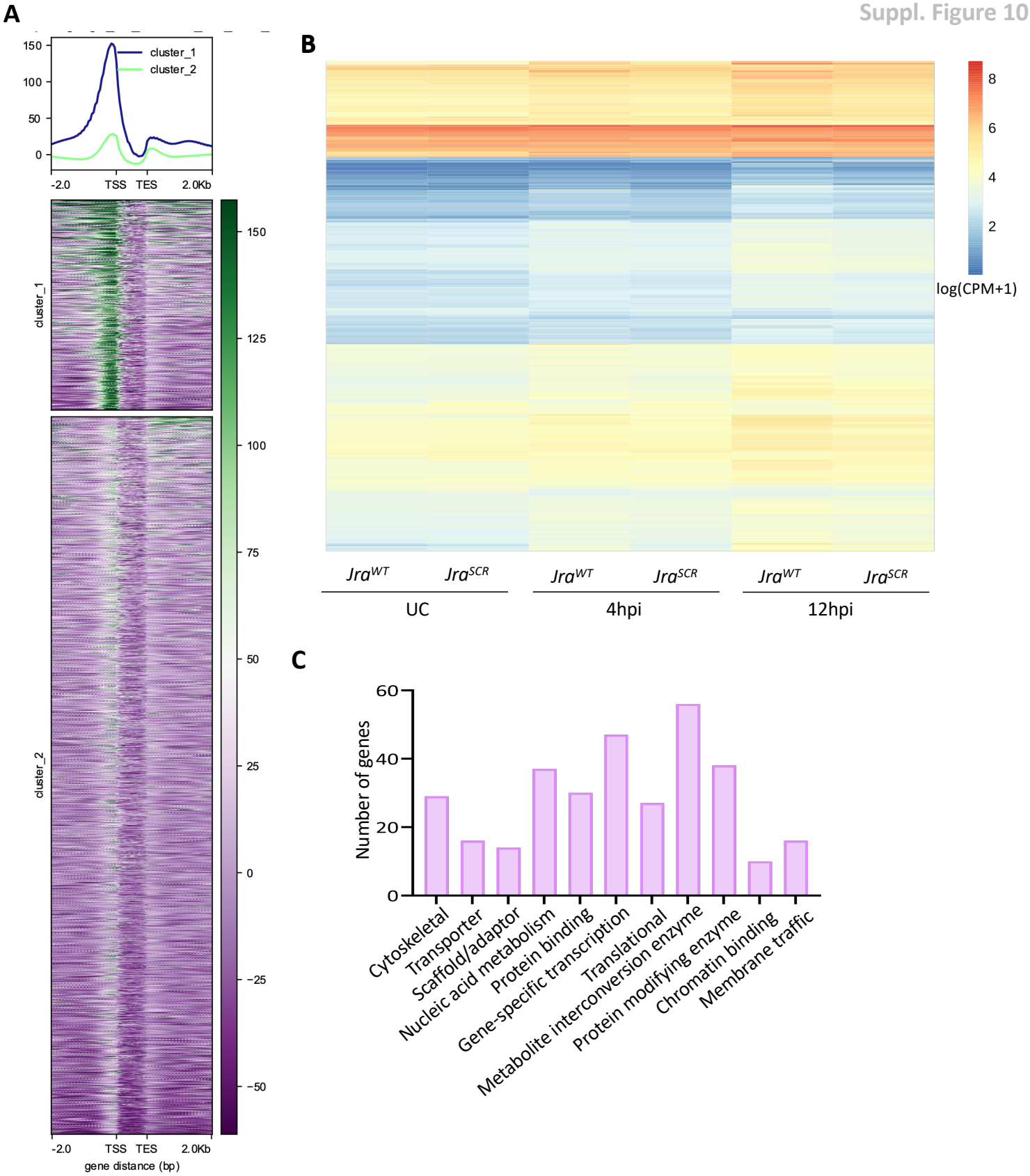

Figure S10: Mapping Jra occupancy on the promoters of differentially expressed genes in *Jra*^{WT} and *Jra*^{SCR}.

A. Heatmap showing occupancy of Jra on the gene body of the differentially expressed genes in *Jra*^{WT} and *Jra*^{SCR}. Cluster 1 represents a set of genes with enriched binding. Heatmap plotted with data extracted from Jra ChIP-seq dataset (ENCSR471GSA) post input (ENCSR908EFA) normalization

B. Heatmap representing the normalised expression counts of genes with enriched Jra binding (cluster 1) on the promoters.

C. GO terms (Panther-Protein class) of genes with enriched Jra binding on the promoters.

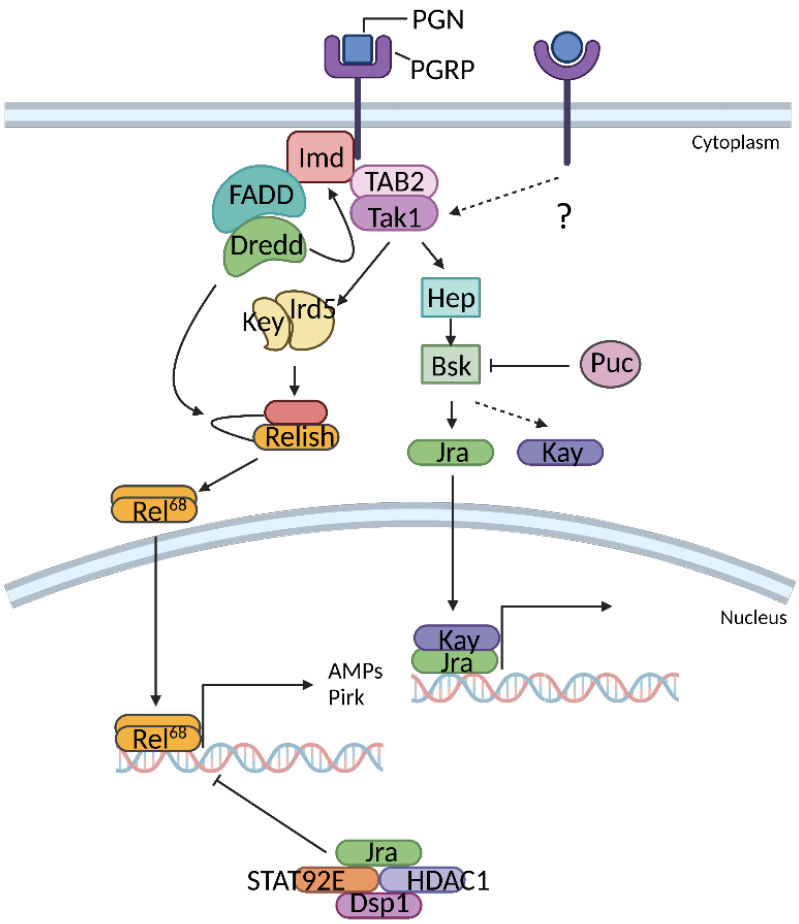

Figure S11: The Imd/JNK pathway in the *Drosophila* immune response.
Upon binding of peptidoglycan (PGN) molecules to the peptidoglycan recognising proteins (PGRPs) presents on the surface of the cell, the Imd pathway gets activated. The adaptor molecule, Imd is cleaved and recruits the TAB2/Tak1 complex. This phosphorylates and activates the IKK complex comprising Key and Ird5. The IKK phosphorylates and activates Rel. Active Rel is cleaved by Dredd and translocates into the nucleus to activate the transcription of antimicrobial peptides (AMPs) and other immune factors. Tak1 parallelly phosphorylates and activates the JNKK, Hemipterous (Hep). Hep activates the JNK, Basket (Bsk) and this inturn activates the AP-1 complex consisting of the dimer Jra and Kay. Jra interacts with HDAC1, STAT92E and Dsp1 to antagonise the activation of *AttA* by Rel.

Supplementary Tables (1-3).

Table S1: XLS files with processed 3' mRNA Sequencing data for the *Jra* knockdown experiment.
Table S2: XLS files with processed 3' mRNA Sequencing data for the Jra^{SCR} experiment.
Table S3: Primer sequences used in this study.